United States
Department of
Agriculture

Forest Service

Pacific Northwest
Research Station

Research Paper
PNW-RP-550
April 2003

Assessing Values of Air Quality and Visibility at Risk From Wildland Fires

Sue A. Ferguson, Steven J. McKay, David E. Nagel, Trent Piepho, Miriam L. Rorig, Casey Anderson, and Lara Kellogg

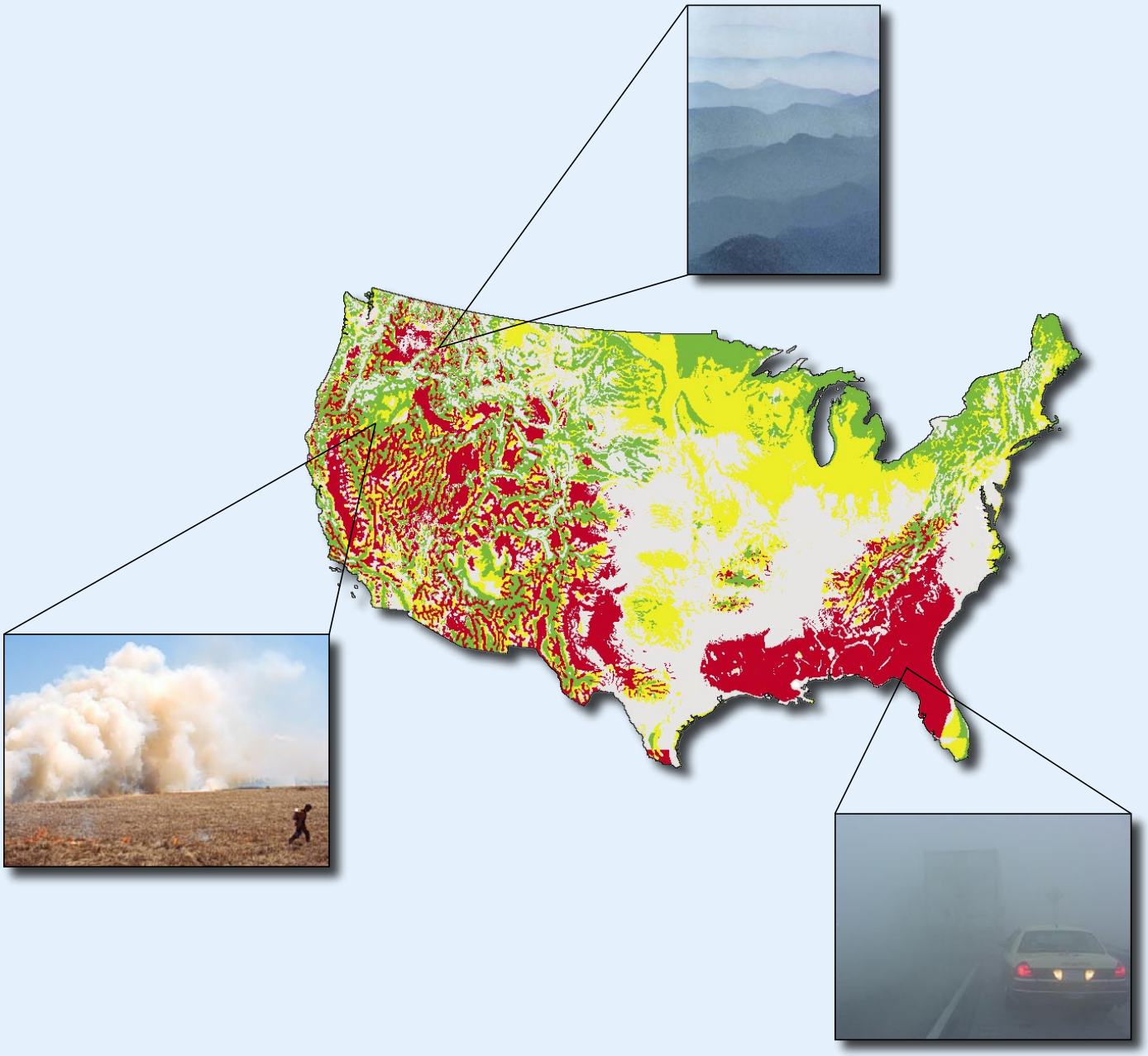

Authors

Sue A. Ferguson is a research atmospheric scientist, **Steven J. McKay** is a statistician, **David E. Nagel** was a geographic information system (GIS) and remote sensing analyst, **Trent Piepho** is a computer scientist, and **Miriam L. Rorig** and **Casey Anderson** are meteorologists, U.S. Department of Agriculture, Forest Service, Pacific Northwest Research Station, Forestry Sciences Laboratory, 400 N 34th St., Suite 201, Seattle, WA 98103; **Lara Kellogg** is a GIS and remote sensing analyst, University of Washington, College of Forest Resources, Seattle, WA 98195. Nagel is currently a GIS analyst with the U.S. Department of Agriculture, Forest Service, Rocky Mountain Research Station, Aquatic Sciences Laboratory, Boise, ID 83702.

Assessing Values of Air Quality and Visibility at Risk From Wildland Fires

Sue A. Ferguson, Steven J. McKay, David E. Nagel, Trent Piepho, Miriam L. Rorig, Casey Anderson, and Lara Kellogg

U.S. Department of Agriculture, Forest Service
Pacific Northwest Research Station
Portland, Oregon
Research Paper PNW-RP-550
April 2003

Final Report for the Joint Fire Science Program

Abstract

Ferguson, Sue A.; McKay, Steven J.; Nagel, David E.; Piepho, Trent; Rorig, Miriam L.; Anderson, Casey; Kellogg, Lara. 2003. Assessing values of air quality and visibility at risk from wildland fires. Res. Pap. PNW-RP-550. Portland, OR: U.S. Department of Agriculture, Forest Service, Pacific Northwest Research Station. 59 p.

To assess values of air quality and visibility at risk from wildland fire in the United States, we generated a 40-year database that includes twice-daily values of wind, mixing height, and a ventilation index that is the product of windspeed and mixing height. The database provides the first nationally consistent map of surface wind and ventilation index. In addition, it is the longest climate record of mixing height in the country. We built the database into an interactive ventilation climate information system that allows users to assess risk based on frequency patterns of poor, marginal, fair, and good ventilation conditions.

Keywords: Ventilation climate information system, ventilation index, air quality, visibility, mixing height, windspeed, wind direction.

Executive Summary

To assess values of air quality and visibility at risk from wildland fire in the United States, we generated a 40-year database that includes twice-daily values of wind, mixing height, and a ventilation index that is the product of windspeed and mixing height. The database provides the first nationally consistent map of surface wind and ventilation index. In addition, it is the longest climate record of mixing height in the country. We built the database into an interactive ventilation climate information system (VCIS) that allows users to assess risk based on frequency patterns of poor, marginal, fair, and good ventilation conditions.

Attributes of the VCIS:

- VCIS is accessed through a Web site at http://www.fs.fed.us/pnw/fera/vent/.
- The data were generated for 40 years at 1200 universal time coordinated (UTC) (morning) and 0000 UTC (afternoon).
- The data cover the United States at 2.5-minute latitude-longitude (about 5 km) spatial resolution in the contiguous 48 states and Hawaii and at 5-km resolution in Alaska.
- Surface winds (10 m above ground level) are generated with a single-level, hydrostatic mesoscale meteorology model.
- Mixing heights are generated by spatially interpolating radiosonde observations; the heights are adjusted to account for intersecting high terrain and local nighttime inversions.
- The ventilation index is a product of surface windspeed and mixing height. Because it uses surface winds instead of higher, trajectory winds, it is a conservative estimate of ventilation potential and most applicable to smoke that remains relatively close to the ground.
- Accuracy of the data has been checked thoroughly, and error information is available on the Web site to help users determine levels of uncertainty.

Risk to values of air quality and visibility from wildland fire:

- The greatest risk occurs in the Southeastern United States where the frequency of poor and marginal ventilation conditions is greatest and the number and density of sensitive receptors are greatest.
- The northern plains and deep valleys in the Western United States also show high risk potential especially during winter and at times during spring and autumn.
- High desert regions show the best potential for good ventilation conditions resulting in the least risk to values of air quality and visibility.
- In all places and at all times of the year, good ventilation conditions and low risk to values of air quality and visibility can occur.
- The likelihood of finding an opportunity for good ventilation on any given day or at any time for any point on the landscape can be determined from frequency plots on the VCIS Web site.
- The year-to-year variability of ventilation index and associated risk in any month and at any point on the landscape can be determined from frequency plots on the VCIS Web site.

Contents

Introduction

With the increasing use of prescribed fire as a way of managing wildland areas in the United States, predicting the potential impacts and assessing risks are becoming more important. Of great concern is the effect of smoke on air quality and visibility. Although few prescribed fires emit enough to violate clean air standards (US EPA 1997), many people are sensitive to slight amounts of smoke, especially if they already experience respiratory problems like emphysema or asthma (Lipsett et al. 1997, Schwartz et al. 1993). Citizen complaints can cause active burning programs to be delayed, redesigned, or even terminated. Also, smoke can severely degrade visibility when combined with other pollutants or moisture. Not only can this detract from scenic vistas, but the degraded visibility from smoke also has been known to cause severe traffic accidents (Achtemeier et al. 1998).

Unfortunately, consistent and timely emission inventories from wildland biomass burning are difficult to obtain and summarize for a national risk assessment. Data on the timing and release rate of emissions, which determine whether smoke will be lofted into the atmosphere or stay close to the ground, are not routinely kept. Lacking detailed and accurate emissions data, it is assumed that a simple index of ventilation potential is sufficient to help determine useful aspects of the risks to air quality and visibility from biomass burning. Because ventilation potential is the product of windspeed and mixing height, its determination is straightforward. Also, current and forecast values of the ventilation index are well known by air quality regulators and are used for managing biomass smoke in many parts of the country (South Carolina Forestry Commission 1996, USDA FS 1976, Utah Administrative Code 2001, Wade and Lunsford 1989).

Developing ventilation potential as a spatial database allows it to be overlain with other elements of risk for a more complete assessment of the impact of prescribed fire in wildland areas of the United States. Certain aspects of ventilation climatology already are well known by air pollution managers. For instance, low mixing heights and poor ventilation are common in coastal areas of the United States where moist marine air increases static stability (Holzworth 1972, Holzworth and Fisher 1979). Poor ventilation also is common everywhere at night when radiative cooling at the surface increases atmospheric stability. What is not known, however, is the probability of poor ventilation on any given day at any selected spot on the landscape. A long time series of high-resolution spatial data can help determine such probabilities.

Because we were tasked to generate a reasonable assessment of risk within 2 years, it was important to develop an accurate database in a short amount of time. We decided that spatial detail was important because most climate summaries are too coarse for application to land management. Also, a long time series was critical to capture naturally varying patterns in climate and to compensate for missing values, and it was important to simulate the diurnal changes. To this end, we generated a 40-year time series at 0000 universal time coordinated (UTC) and 1200 UTC each day.[1]

[1] The times, 0000 UTC and 1200 UTC, correspond to standard time in Greenwich, England, or Greenwich Mean Time (GMT), and are called synoptic times because measurements collected all over the world occur simultaneously at these times to provide a consistent synopsis of the weather. It is morning in most of the United States at 1200 UTC and afternoon of the preceding day at 0000 UTC. For example, 1200 UTC on December 1st is 4 a.m. (04:00) December 1st in San Francisco, whereas 0000 UTC on December 1st is 4 p.m. (16:00) November 30th in San Francisco. The letter Z, which is short for Zulu, is used as a nickname for UTC (e.g., 0Z and 12Z).

The generated values of wind, mixing height, and ventilation index cover the United States at a horizontal grid spacing of 2.5 minutes latitude-longitude (about 5 km), except Alaska where the grid spacing is fixed at 5 km × 5 km map projections (see app.1).

Because we needed to generate the high-resolution climate information in a short time, relatively simple tools were used to derive data values, and several simplifying assumptions were made. We tried to maintain physical reasonableness by checking our results frequently against observations and common knowledge. Any time data are derived, however, whether by spatially interpolating observations or by using physical models, accuracy and reliability are influenced. Therefore, details on the derivation process, assumptions, and methods of smoothing and parameterization are given to help users evaluate uncertainty in subsequent risk assessments. The first few sections of this report explain in detail the technical development of each meteorological component: development of the surface wind fields, mixing height derivation, and calculation of the ventilation index. We have highlighted key elements at the end of each section that may be of value to land managers.

After developing the spatial database, we assessed values of air quality and visibility at risk from wildland fire by grouping the ventilation index into large areas representing regional airsheds. The variation in space and time within each airshed and among individual airsheds also is discussed, with supporting data shown in appendix 3.

With over 100 gigabytes of data we cannot summarize everything effectively in a manuscript. Therefore, we made all the data and documentation available through a Web site that includes an interactive map (http://www.fs.fed.us/pnw/fera/vent/). The interactive ventilation climate information system (VCIS) allows users to map monthly values of ventilation index with sensitive receptors, natural and political boundaries, and topography. In addition, users can zoom or print maps, and it may be possible to import Web-generated maps into their own geographic information system (GIS) application. At any time, a summary of daily, monthly, and annual statistics for each variable at any point can be obtained by a simple mouse click. Appendix 2 explains how to interpret the VCIS map products and graphs. A guide to the VCIS Web site is given in appendix 4.

Wind

To generate surface winds, we modified the single-level hydrostatic flow model of Danard (1977), Dempsey (1985), and Mass and Dempsey (1985). Various versions of the model have successfully simulated sea-land breezes in Israel (Alpert 1988, Alpert and Getenio 1988, Alpert et al. 1988), and orographic flow fields for alpine precipitation forecasting (Speers and Mass 1986). We modified the model to accommodate a spatially varying lapse rate and to run on a message-passing parallel computing platform. In addition, we modified the finite difference calculations to make them more stable and increase success rate in converging to a physically reasonable solution. We call our modified version of the Danard, Mass, and Dempsey model WINFLO. We chose to use WINFLO to generate surface winds over the large domain of the United States and the long, 40-year period because of its rapid computation, reasonably accurate output, and success in a variety of applications.

Even though we had a high-speed, parallel computing platform of forty 850-megahertz processors to run the model, for twice daily simulations over 40 years we needed to turn off the heating and cooling component within WINFLO to speed computations. This allowed us to complete the simulations within months instead of years. The heating and cooling component is designed to capture heat fluxes between the ground surface and atmosphere. Without the component, resulting winds are considered applicable to

diurnally neutral times near sunrise and sunset. This means that the model will not resolve sea breezes or slope flows if they are not reflected in the 85 kiloPascal (kPa) heights and temperatures at 1200 UTC or 0000 UTC.

WINFLO uses sigma coordinates (terrain-following surfaces of constant pressure), with the single-layer sigma surface representing about 10 m above ground level (agl). Only two classes of land surface are used, forested land and open water, with drag coefficients of 0.015 and 0.0014, respectively. Although we did not find significant differences in model results when we changed the drag coefficient over land during tests in Oregon, we expect that the coarse land-use categories may cause the model to underestimate surface winds over broad flat areas and grasslands.

As a hydrostatic model, WINFLO functions best when vertical motions are small compared to horizontal motions. Hydrostatic assumptions typically are inappropriate for horizontal scales less than about 5 km and during strongly dynamic events such as thunderstorms and gusting fronts. To accommodate the hydrostatic assumption, we kept the horizontal grid resolution near 5 km and created an upper limit of 8 °C/km and lower limit of 3.5 °C/km for the lapse rate. Lapse rates were calculated between the 85 kPa and 50 kPa vertical levels. Observed values rarely exceeded 8 °C/km but occasionally were less than 3.5 °C/km. This forces some smoothing that would cause gusty surface winds to be underestimated by the model. This condition does not affect strong, sustained storm winds that are successfully simulated by WINFLO.

The upper-boundary initialization data were from the National Centers for Environmental Prediction (NCEP) reanalysis package (Kalnay et al. 1996). We chose to initialize the model with data from the 85 kPa level. This height usually is about 1500 m above sea level (asl), which is below the height of many mountain ranges in the Western United States. At the resolution of the reanalysis data, however, the western mountains are represented as highly smoothed undulations, and the 85 kPa height seems to reasonably represent conditions above major orographic influences while reflecting surface conditions. For example, we simulated winds over the Sawtooth Mountains in Idaho, which consistently rise above 2500 m asl, with both an 85-kPa reference height and a 70-kPa reference height (about 3000 m asl). When comparing model output with observations, including many high-elevation wind measurements from the interagency remote automated weather stations (RAWS) network (USDI 1995), we found little difference in model performance between the two tests except that the model performed slightly better at turning winds through the terrain patterns when using data from the 85-kPa reference level than when using data from the 70-kPa level. Also, results from the 85-kPa height were consistently better at lower-elevation sites.

Observed Versus Modeled Wind

Surface winds are strongly influenced by small-scale undulations in terrain and land cover. Therefore, wind observations that are measured by anemometers are influenced by, and represent, conditions below the resolution of the model terrain and land-use grids and may not represent the larger scale windfield. In addition, anemometers usually have stall speeds that prevent accurate recording when windspeeds are below about 1 m/s; they can be placed poorly in relation to buildings, towers, and other instruments; and often they are poorly maintained. Therefore, it can be difficult to compare model-derived winds with observations. In each region, however, we asked local climatologists to review the wind maps to determine if patterns appeared reasonable.

The observations we selected for comparison came from National Oceanographic and Atmospheric Administration (NOAA) National Weather Service primary observing stations (National Climatic Data Center 1997, National Renewable Energy Laboratory 1992). Data from local and regional networks, such as the interagency RAWS network (USDI 1995), did not have adequate quality or consistency for model verification over the entire country and in all seasons.

To compare modeled winds with observed winds, we qualitatively analyzed general flow patterns, developed grouped statistics, and compared observed to modeled winds at each observation location. Figure 1 is an example of one of our qualitative plots that illustrates how general flow patterns compare with observations at specific times in a small region centered over southern Idaho and northern Utah. During the afternoon (fig. 1a), observed winds at Boise, Idaho (BOI), and Salt Lake City, Utah (SLC), were from the northwest at about 10 m/s. Modeled winds in the Boise area were generally from the northwest at about 8 m/s but turning south-southeast away from the central valley. Modeled winds over Salt Lake City were generally north-northwesterly at about 8 m/s.

During the morning (fig. 1b), both modeled and observed winds at Boise became slower and turned southeasterly. Although observed winds over Salt Lake City appeared from due north in the morning, modeled winds around the area were variable from southeast to northeast. Away from the observation points, flow patterns appear consistent with typical diurnal wind patterns (up valley during the late afternoon and down valley in the early morning) with expected channel flow through gaps and valleys. Therefore, although minor inconsistencies occur at the observation points, the general flow pattern is physically consistent and realistic. Other similar subjective comparisons resulted in the same conclusions.

Besides subjective comparisons, we calculated error statistics for each season. Although statistical errors may seem high, it does not mean that the models are grossly inaccurate. Anemometers respond to very subtle features of land cover and terrain that are below the resolution of model grid spacing. Also, there may be differences in timing or errors in the observations themselves that can cause large differences. Therefore, statistical error summaries are more useful in highlighting inherent biases and tracking spatial or temporal inconsistencies rather than providing an exact evaluation of accuracy. We calculated differences in windspeed, wind direction, and vector wind. Vector winds are simply the east-west and north-south components of a wind vector whose length is represented by speed. Vector wind differences (*vwd*) account for differences in speed and direction simultaneously and are calculated as:

$$vwd = \sqrt{(U_m - U_o)^2 + (V_m - V_o)^2} \ ,$$

where $U = W_s \times \sin(W_d)$, and $V = W_s \times \cos(W_d)$, with W_s = wind speed, W_d = wind direction, and the subscripts m = modeled and o = observed. Several statistics were calculated for each season—winter (December, January, February), spring (March, April, May), summer (June, July, August), and autumn (September, October, November)—as follows:

1. Mean error is the average of modeled minus observed values. It shows if there are consistent biases but allows positive and negative errors to cancel each other out.

2. Mean absolute error is the average of the absolute value of modeled minus observed values. It shows the magnitude of difference.

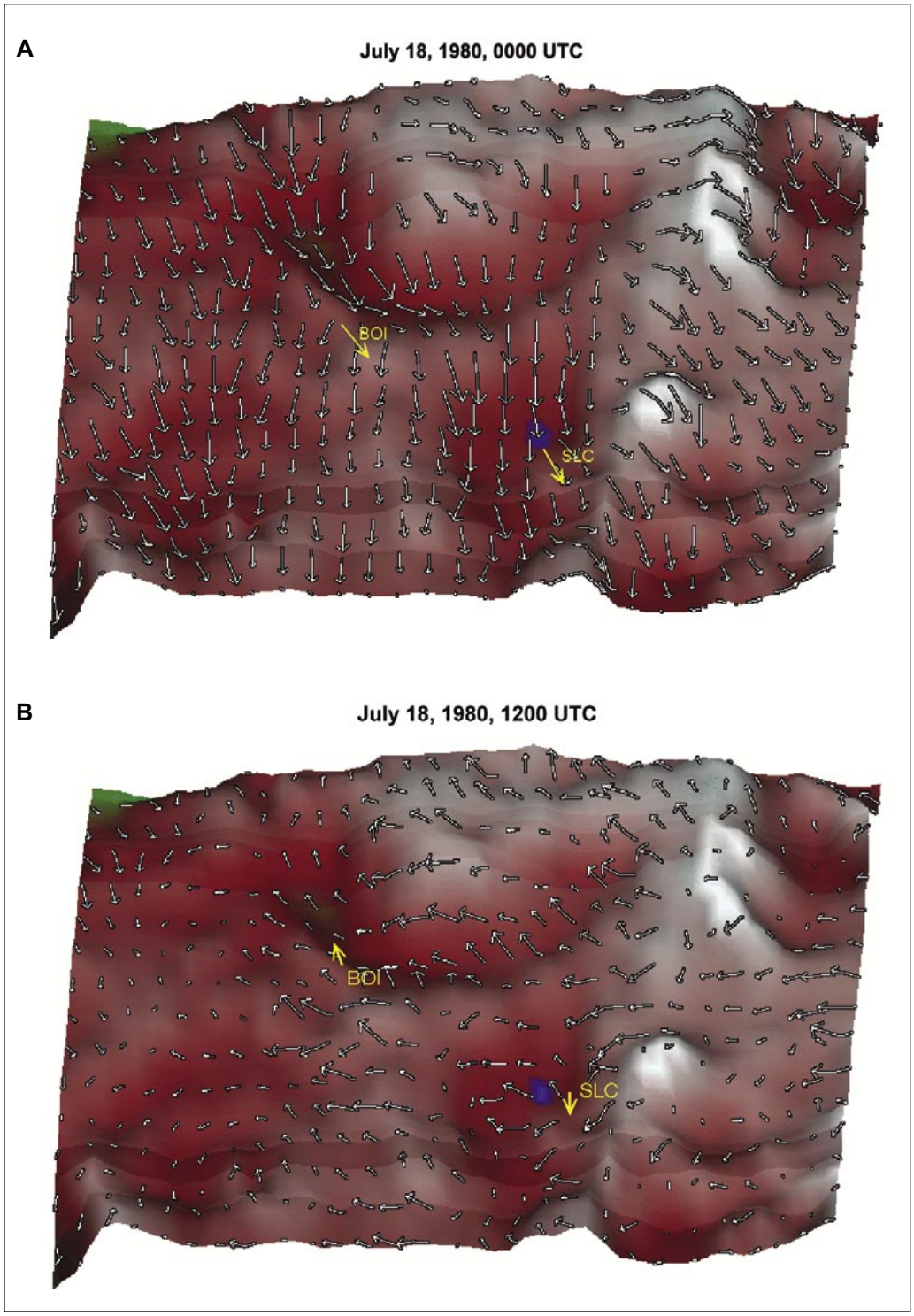

Figure 1—Modeled surface wind patterns over northern Utah and southern Idaho on 18 July 1980 for (A) 0000 universal time coordinated (UTC) and (B) 1200 UTC. Observed winds at Salt Lake City, Utah (SLC), and Boise, Idaho (BOI), are shown in yellow.

3. Root mean square (RMS) error is the square root of the difference between the square of the modeled value and the square of the observed value. This causes large differences to be weighted more than small differences. The lower the RMS error, the fewer large differences. If the model and observed values were identical, the RMS error would be zero.

Examples of some statistical results are shown in tables 1 and 2. Ten years of modeled surface wind in the Northwestern United States from WINFLO at 2.5-minute latitude-longitude (about 5 km) spatial resolution is compared with about 2 years of modeled surface winds from the Northwest real-time MM5 meteorological model (Ferguson 2001) for a subset of the same domain at 4-km spatial resolution. The MM5 surface winds were derived from its lowest sigma level in 1998, which was about 40 m agl then adjusted to 10 m agl.[2] For this comparison, winds were represented in knots (knots x 0.515 = m/s).

Negative mean errors in windspeed for WINFLO indicate that modeled winds frequently may be slower than observed winds. Positive mean errors in MM5 suggest that modeled winds frequently may be higher than observed winds. Slowest biases in both models occur during spring and summer. This may be due to the inability of models to capture gusty winds associated with strong convection. Slow biases in WINFLO average less than -1 knot (-0.5 m/s) at most times in most seasons. During the afternoon, however, biases average about -4 knots (-2 m/s) in spring and summer, and about -2 knots (-1 m/s) in autumn.

Mean absolute errors in direction for WINFLO ranged from about 56 degrees in spring afternoons to 78 degrees in summer mornings, whereas MM5 errors ranged from about 48 to 66 degrees. Mean absolute errors in WINFLO's speed ranged from 3.2 knots (1.6 m/s) in summer mornings to 4.9 knots (2.5 m/s) in spring afternoons, whereas MM5 errors ranged from 3.0 knots (1.5 m/s) to 5.4 knots (2.8 m/s). The RMS errors in direction range from about 73 to 89 degrees for WINFLO and about 65 to 84 degrees for MM5, suggesting that large differences between modeled and observed direction are possible. The RMS errors in speed range from 4.1 knots (2.1 m/s) to 6.4 knots (3.3 m/s) in WINFLO and from 5.1 knots (2.6 m/s) to 7.0 knots (3.6 m/s) in MM5. Vector wind differences from WINFLO (6.8 to 9.4 knots) were in the same range as those from MM5 (6.0 to 10.8 knots).

Our most extensive error analysis was accomplished by plotting the frequency of modeled and observed windspeed and direction at each observation location (fig. 2). Also included are maps surrounding each observation station of the terrain elevation at 90-m resolution as shaded relief, terrain elevation at model resolution (5 km), and land cover class at 90-m resolution. This allows the user to distinguish whether differences between modeled and observed winds at that location are due to smoothing of terrain and land use in the model or caused by other model constraints.

Plots were generated for each month and each synoptic time period, allowing for examination of seasonal and diurnal performance. Directional difference is determined by subtracting each observation from its corresponding modeled value. When observed winds are less than 1 m/s, however, they and the corresponding modeled winds are excluded from difference calculations to account for the threshold windspeed, or stall speed, of most anemometers. Differences between modeled and

[2] For a description of the Northwest real-time model and verification methods see http://www.atmos.washington.edu/mm5rt/.

Table 1—Error statistics between modeled and observed winds in the Northwest region from WINFLO model with 28 observations in 10 years

			All observed windspeeds				Observed windspeeds >5 knots			
	Hour[a]	Season	Mean error	Mean absolute error	Root mean square error	Count	Mean error	Mean absolute error	Root mean square error	Count
			Degrees				*Degrees*			
Direction	0Z	Winter	4.361	63.692	82.301	21,005	1.681	52.425	71.320	14,645
		Spring	.466	55.884	73.037	24,684	.573	52.490	69.297	21,994
		Summer	-10.184	58.935	76.089	15,404	-10.378	56.357	73.460	13,902
		Autumn	.291	59.934	77.798	12,341	.370	53.132	70.962	9,783
	12Z	Winter	5.037	69.840	88.102	20,406	-1.597	53.383	73.009	11,899
		Spring	-1.339	70.547	87.818	23,914	-1.930	59.827	79.007	14,243
		Summer	-5.131	77.521	94.091	14,875	-3.517	69.711	89.182	8,296
		Autumn	3.395	71.713	89.002	11,894	1.715	57.278	76.852	6,673
			Knots[b]				*Knots*[b]			
Speed	0Z	Winter	-.697	3.879	5.185	21,005	-2.275	4.027	5.458	14,645
		Spring	-3.878	4.940	6.368	24,684	-4.596	5.213	6.635	21,994
		Summer	-3.482	4.807	6.131	15,404	-4.170	4.962	6.303	13,902
		Autumn	-2.023	3.966	5.124	12,341	-3.180	4.209	5.379	9,783
	12Z	Winter	.976	4.010	5.257	20,406	-1.148	3.772	5.171	11,899
		Spring	-.093	3.437	4.389	23,914	-2.064	3.441	4.402	14,243
		Summer	-.222	3.245	4.105	14,875	-2.389	3.273	4.091	8,296
		Autumn	.611	3.635	4.621	11,894	-1.505	3.479	4.476	6,673
Vector wind differences	0Z	Winter	6.931	6.931	8.175	21,005	7.586	7.586	8.880	14,645
		Spring	8.197	8.197	9.371	34,684	8.562	8.562	9.711	21,994
		Summer	8.359	8.359	9.424	15,404	8.600	8.600	9.671	13,902
		Autumn	7.171	7.172	8.263	12,341	7.659	7.659	8.748	9,783
	12Z	Winter	6.849	6.849	8.013	20,406	7.424	7.424	8.726	11,899
		Spring	6.167	6.169	7.077	23,914	6.809	6.809	7.732	14,243
		Summer	5.968	5.968	6.814	14,875	6.770	6.770	7.593	8,296
		Autumn	6.279	6.279	7.241	11,894	6.933	6.933	7.939	6,673

[a] 0Z = 0000 universal time coordinated (UTC); 12Z = 1200 UTC.

[b] Knots × 0.515 = meters per second.

Table 2—Error statistics between modeled and observed winds in the Northwest region from MM5 model with over 1,000 observations in about 2 years

			All observed windspeeds				Observed windspeeds >5 knots			
	Hour[a]	Season	Mean error	Mean absolute error	Root mean square error	Count	Mean error	Mean absolute error	Root mean square error	Count
			Degrees				*Degrees*			
Direction	0Z	Winter	26.978	59.887	77.619	2,981	25.720	46.892	63.013	14,645
		Spring	4.777	58.341	76.342	6,953	11.081	43.980	62.705	21,994
		Summer	.248	63.220	80.764	7,707	12.311	46.729	65.347	13,902
		Autumn	10.895	66.078	83.827	6,855	15.078	44.357	60.592	9,783
	12Z	Winter	20.188	60.575	79.072	3,665	19.422	45.566	62.642	11,899
		Spring	7.170	54.434	72.172	9,235	9.631	46.528	63.825	14,243
		Summer	10.993	47.877	64.711	8,955	13.251	40.893	56.423	8,296
		Autumn	9.262	57.988	76.518	7,858	11.832	42.985	60.050	6,673
			Knots[b]							
Speed	0Z	Winter	2.931	5.359	6.974	3,050				
		Spring	1.260	3.622	4.685	7,081				
		Summer	1.920	3.654	4.633	7,790				
		Autumn	2.568	4.318	5.531	6,946				
	12Z	Winter	2.125	4.808	6.429	3,748				
		Spring	-.884	3.379	4.453	9,523				
		Summer	-.607	3.078	4.127	9,230				
		Autumn	.586	3.370	4.596	8,004				
Vector wind differences	0Z	Winter	9.122	9.122	10.814	3,050				
		Spring	5.623	5.623	6.841	7,081				
		Summer	5.523	5.523	6.054	7,796				
		Autumn	6.324	6.324	7.595	6,946				
	12Z	Winter	8.084	8.084	9.746	3,748				
		Spring	6.014	6.014	7.138	9,523				
		Summer	5.363	5.363	6.396	9,230				
		Autumn	5.574	5.574	6.978	8,004				

[a] 0Z = 0000 universal time coordinated (UTC); 12Z = 1200 UTC.

[b] Knots × 0.515 = meters per second.

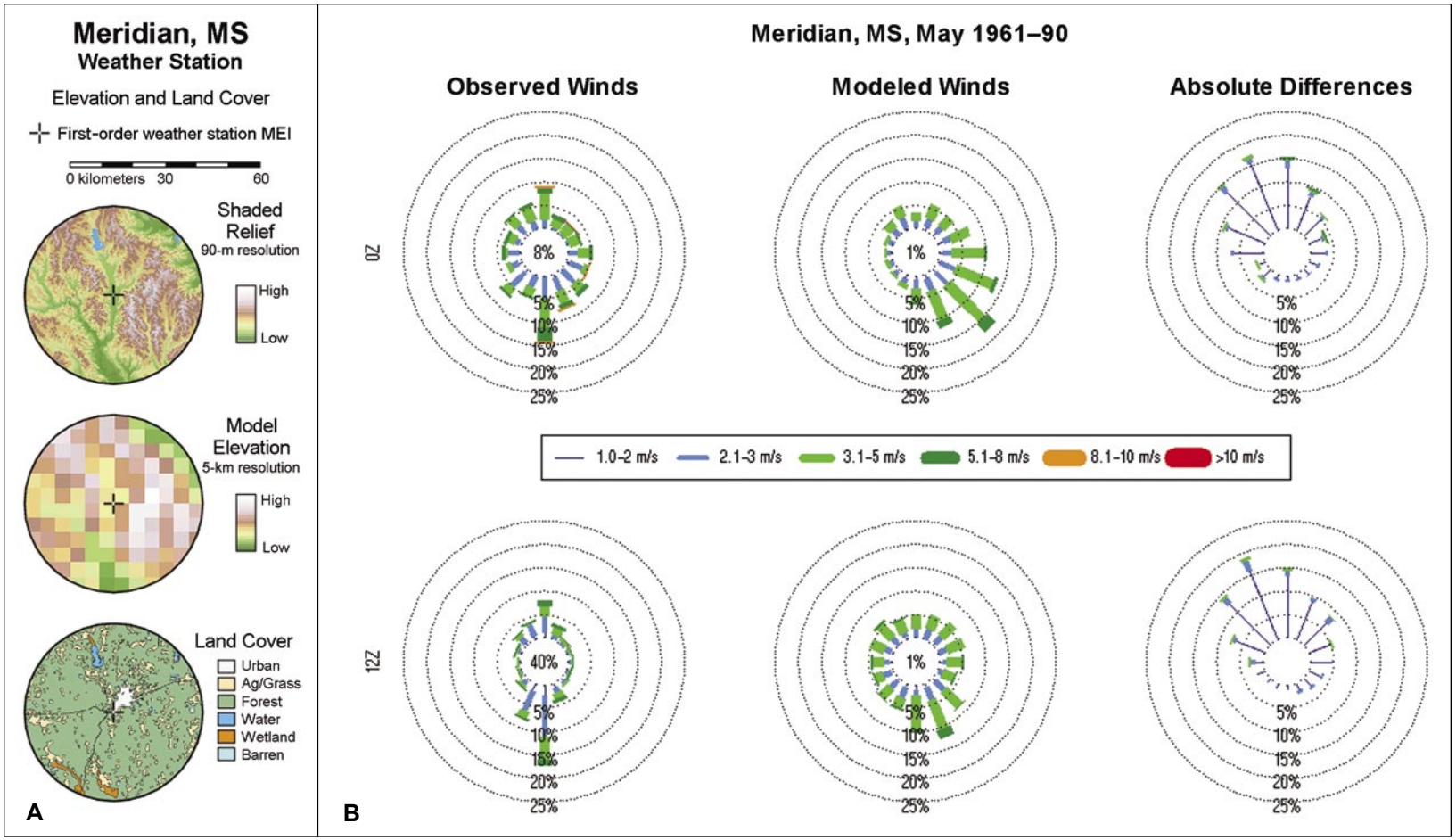

Figure 2—Modeled versus observed winds at Meridian, Mississippi (MEI), in May 1961 to 1990: (A) station location (cross hair) is shown with shaded relief, model elevation, and land cover, and (B) polar plots of observed and modeled winds and polar plots of absolute differences for both 0000 UTC (top row) and 1200 UTC (bottom row). See appendix 2 for an explanation of polar plots.

observed windspeeds are presented as positive values, not distinguishing between overestimation and underestimation, hence the term “absolute difference.” Difference in speed is represented by line thickness and uses the same speed classes as wind roses (see app. 2), except that differences less than 1 m/s are not a separate category, causing the thinnest line segments to represent all windspeed differences less than 2 m/s. Difference in direction is represented by the angle at which a ray radiates out from the center of the plot. Straight up indicates essentially no difference (within 11.25 degrees). An angle of 90 degrees indicates that the modeled winds differ from the observed winds by 90 degrees in the clockwise direction (i.e., an observed direction of northeast and a modeled direction of southeast).

Comparing the polar plots of differences to terrain and land use around the observation station helps to determine whether the model is failing because of its simplified physics and numerical schemes or because its terrain and land use are not representative of local features affecting the anemometer measurement. For example, Meridian, Mississippi, lies in a narrow valley that is oriented north to south (fig. 2). The valley causes observed winds to be funneled primarily from the north or south directions. The elevation from the 2.5-minute latitude-longitude model, however, does not resolve the narrow valley very well. This causes modeled surface winds to be controlled by larger topographic features and upper level conditions, such as when modeled wind directions prevail from the southwest in May. Although absolute differences between modeled and observed winds at Meridian show only small speed differences, there is a frequent directional bias of 15 to 30 degrees in May, likely caused by the differences between actual and modeled topography.

In general, the model performed very well with respect to both windspeed and wind direction. The two land-use categories (land and water) in the model, however, tend to bias toward rough terrain (forested and mountainous). This causes strong winds (>8 m/s) to be underestimated over broad flat areas and grasslands. Also, the smoothed-model terrain appears to cause a modest directional bias of less than 45 degrees in either the clockwise or counterclockwise direction. Finally, restrictions on the model lapse rate (temperature difference with height) and omission of radiative heating appear to cause poor model performance in some months at western arid sites.

Overlapping Domains

The hydrostatic assumption and other methods of simplifying the physics cause the numerical processing in WINFLO to have difficulty converging to a solution when there is a sharp pressure ridge or trough in the modeling domain. To maximize convergence opportunities, we divided the country into overlapping regional domains (fig. 3). Each domain was selected to encompass terrain features that may influence pressure-gradient forces and minimize potential edge effects. Because the numerical processing never yields exactly the same value, we merged model runs from overlapping domains with a simple weighted-average algorithm. The scheme used weights proportional to the distance from the boundary of the domain. A grid cell on the boundary receives a weight of zero, a grid one cell away from the boundary receives a weight of one, and so on. Windspeed and direction were averaged separately then combined to give the final wind vector. Windspeed was averaged as a typical weighted mean. To calculate the average wind direction, weighted means were found for the cosine (east-west) and sine (north-south) components of the wind direction. The resulting direction is the arctangent of the mean north-south component divided by the mean east-west component. For example, if a specific grid cell in an overlap region was located 17 grid cells from the edge of the Northwest (NW) domain with a speed of 3.0 m/s from

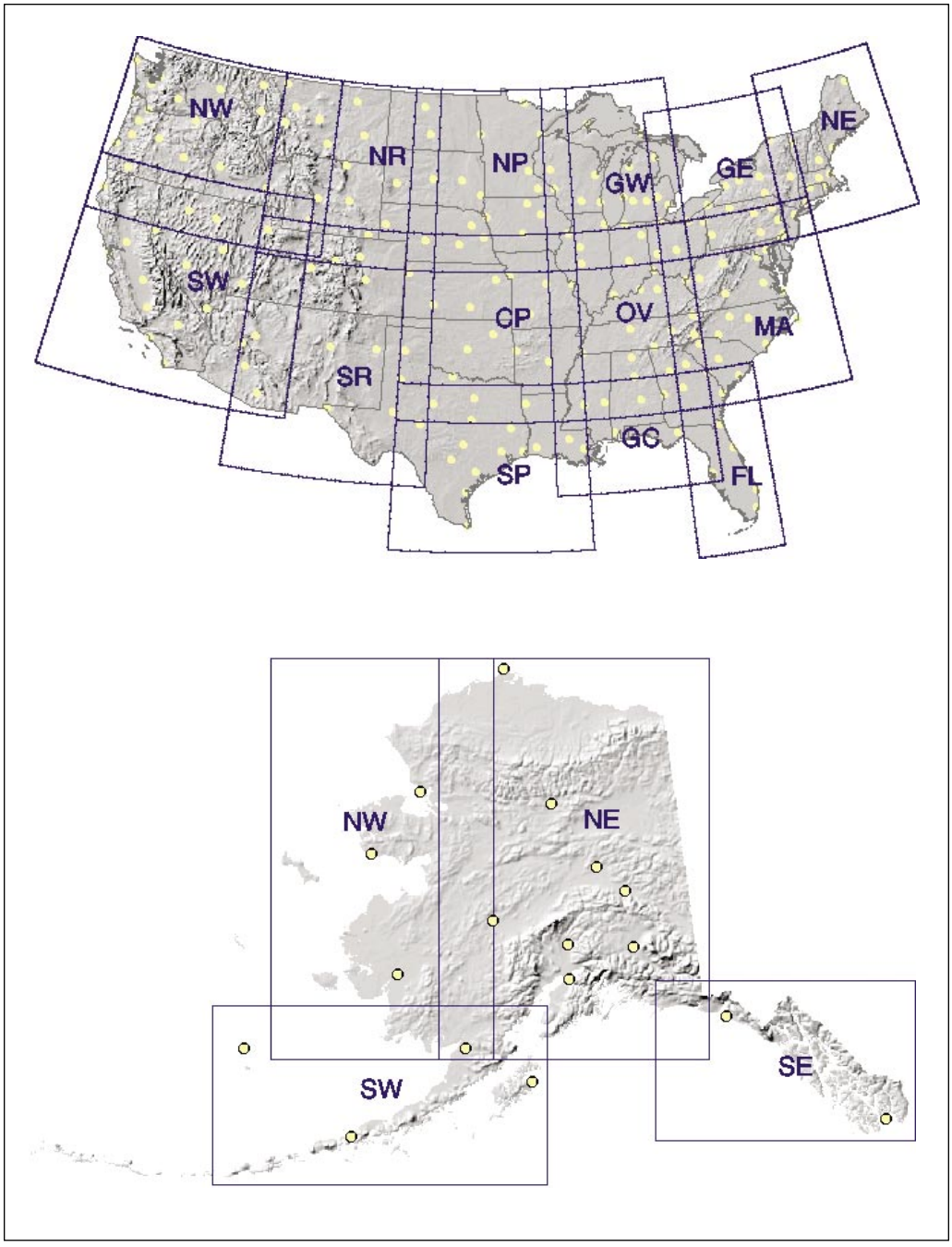

Figure 3—Domains used for modeling surface wind in the contiguous 48 states and Alaska. Hawaii was modeled in a single domain. Dots indicate observation locations that were used for verification.

180 degrees and 75 grid cells of the edge of the Northern Rockies (NR) domain with a speed of 3.5 m/s from 170 degrees, its resulting speed value would be 3.4 m/s and its resulting direction value would be 171.8 degrees:

$$W_s = \frac{(30 \times 17) + (35 \times 75)}{(17 + 75)} = 3.41 \text{ m/s}$$

$$W_d = \arctan\left[\frac{(\sin 180^\circ \times 17) + (\sin 170^\circ \times 75)}{(\cos 180^\circ \times 17) + (\cos 170^\circ \times 75)}\right] = 171.8^\circ$$

Although the small domains helped reduce the amount of missing wind values, there still were times when the model did not converge. Table 3 summarizes the percentage of time that WINFLO failed to converge in each domain for each month. This indicates the number of times wind data were not generated and unavailable for ventilation index calculations. WINFLO clearly had the most difficult time in the Mid Atlantic (MA) and New England (NE) regions during the winter. This may be due to the vigorous storms that can occur in those regions and the difficulty of convergence when there are steep gradients in the pressure field. Also, there is some indication that WINFLO has difficulty with storms moving into the domain from the east,[3] which is possible on the eastern seaboard.

Because several domains were merged together to generate a national coverage of wind, we closely examined winds in the overlapping regions to evaluate potential edge effects. We always found model-generated winds from one domain to be reasonably consistent with winds generated from the overlapping domain. For example, Medford, Oregon, and Winnemucca, Nevada, are two stations in the overlap zone between the NW and Southwest (SW) domains, with Winnemucca near the center of the overlap zone and Medford near the northern border of the SW domain. The two model runs agree more closely at the central site (Winnemucca) but do not differ grossly at the border site (Medford) (fig. 4). Because data near the border of a domain receive less weight when the domains are merged, the edge effect becomes negligible in the merged data.

Observations in each overlap zone were used to check for consistency between model output from individual domain runs and calculated overlap values. In general, no accuracy was lost by using the overlap merging algorithm, and realistic national patterns of wind resulted.

WINFLO-XY for Alaska

The numerical routines in WINFLO assume relatively square grid cells even though they are based on latitude-longitude coordinates. This assumption appears to work well in midlatitudes, where the model has been most successfully used, but is not valid in high-latitude regions, above about the 52nd parallel, such as Alaska. We created a constant distance version of WINFLO (WINFLO-XY) to apply in the Alaska region and ensured that it produces results similar to the original WINFLO in midlatitudes. Whereas the contiguous 48 states and Hawaii have grid resolutions of 2.5 minutes latitude-longitude, which is about 5 km, the Alaska grid cells are fixed at 5 km on a side. Digital elevation model (DEM) data were aggregated and projected (see app. 1) to match the grid size in each domain, providing the lower boundary of WINFLO domain.

[3] Speers, P. 1999. Personal communication. Meteorologist, USDA Forest Service, Northwest Weather and Avalanche Center, 7600 Sandpoint Way NE, Seattle, WA 98115.

Table 3—Percentage of missing wind data for each regional WINFLO modeling domain

Domain	January	February	March	April	May	June	July	August	September	October	November	December
							Percentage					
Contiguous 48 states:												
Central Plains (CP)	0.36	0.27	0.12	0.08	0	0	0	0	0	0	0	0.08
Florida (FL)	6.69	7.50	5.73	4.08	.97	.42	0	0	.33	1.05	3.21	5.27
Great Lakes East (GE)	2.22	2.37	1.69	.88	.73	.17	.04	.12	.25	.25	.93	2.11
Great Lakes West (GW)	6.77	5.63	3.59	3.46	2.22	1.04	.32	.40	1.21	1.69	3.08	4.81
Gulf Coast (GC)	1.73	2.50	1.17	.75	.28	.08	0	0	0	.25	.97	1.77
Mid Atlantic (MA)	12.26	13.39	10.52	6.58	4.92	2.17	.81	.77	.83	3.00	4.77	9.62
New England (NE)	10.89	11.79	10.04	9.54	6.94	2.42	1.13	1.25	5.25	5.40	7.09	8.95
Northern Plains (NP)	.77	.76	.12	.08	0	0	0	0	0	.04	.08	.46
North Rockies (NR)	1.49	.89	.36	0	0	0	0	0	0	.04	.25	.72
Northwest (NW)	.81	.31	.20	.08	0	0	0	0	.04	.13	.80	.30
Ohio Valley (OV)	.16	.13	.08	.08	0	0	0	0	0	0	0	.08
Southern Plains (SP)	.93	1.12	.56	.25	.08	0	0	0	0	.04	.30	1.22
South Rockies (SR)	.16	.13	.04	.04	0	0	0	0	0	0	0	.08
Southwest (SW)	0	.04	0	0	0	0	0	0	0	0	0	0
Alaska:												
Southeast (SE)	10.40	7.45	5.24	2.91	2.90	3.16	2.45	2.09	1.70	2.05	5.75	7.33
Northeast (NE)	2.94	4.06	3.10	1.00	.40	1.33	1.41	1.08	.54	.60	1.41	3.26
Southwest (SW)	19.26	20.76	17.18	14.57	10.82	11.52	10.59	9.58	6.28	9.58	15.66	19.39
Northwest (NW)	19.75	20.75	22.25	17.58	12.94	17.00	13.58	9.63	6.58	9.75	17.54	22.90
Hawaii	1.81	1.83	1.00	1.08	.88	.70	1.29	.56	.54	.80	.95	2.17

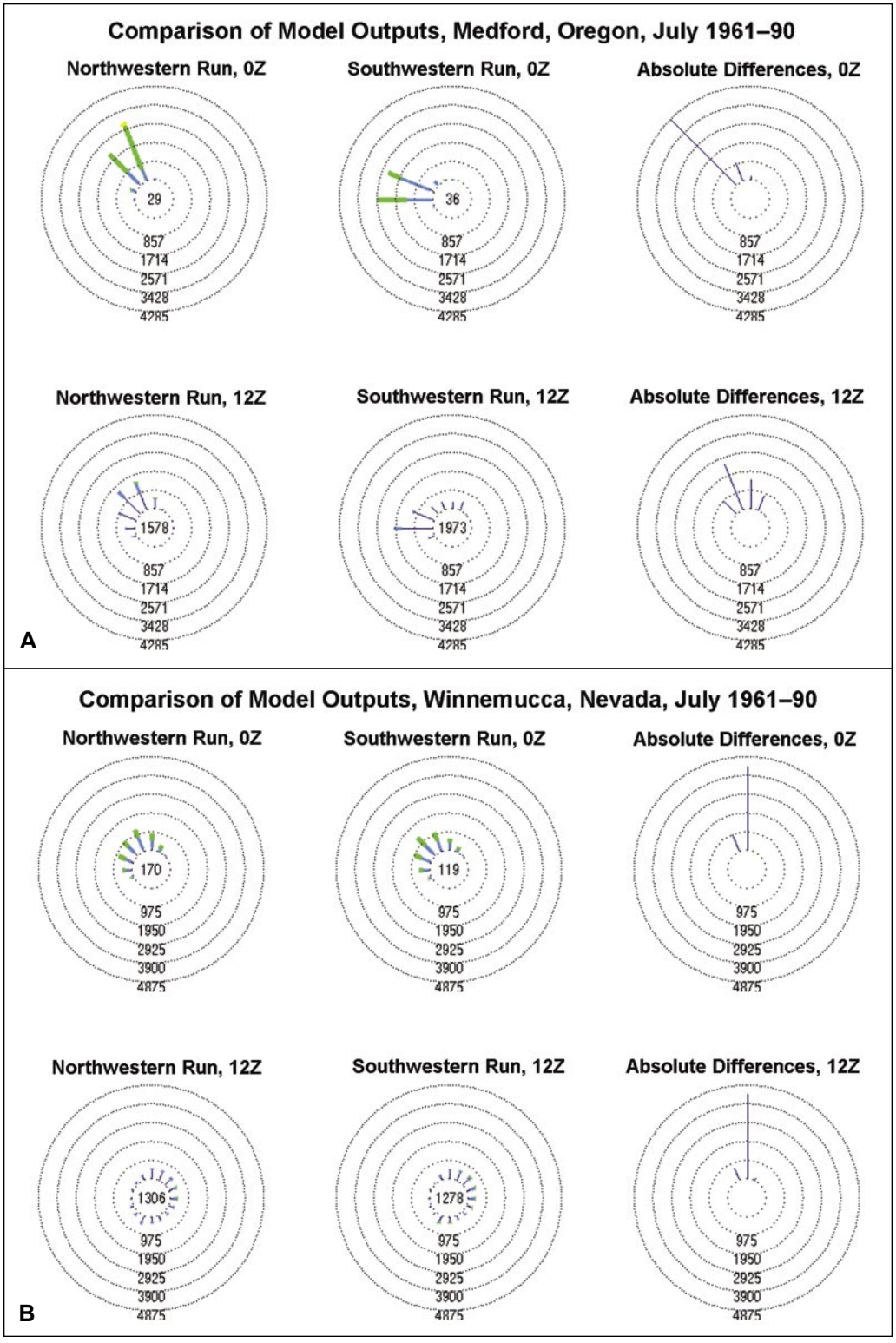

Figure 4—Absolute differences between modeled winds as derived from the Northwestern and Southwestern domains at (A) Medford, Oregon, and (B) Winnemucca, Nevada. 0Z and 12Z correspond to 0000 universal time coordinated (UTC) and 1200 UTC, respectively.

Key Elements of Wind

- The WINFLO surface wind model is computationally efficient, reasonably accurate, and has shown success in a variety of applications.
- Surface winds apply to conditions near sunrise and sunset, even though the morning (1200 UTC) and the afternoon (0000 UTC) initialization times do not always coincide with sunrise and sunset.
- Surface windspeeds over broad, flat areas and grasslands may be underestimated at times.
- Gusty surface winds may be underestimated by WINFLO, but the model successfully simulates strong, sustained storm winds.
- The choice of the 85 kPa (about 1500 m asl) height as an upper initialization field appears reasonable, even over high-elevation mountains.
- Surface windspeeds from WINFLO are consistently slower than observed, especially during the afternoon in spring and summer.
- WINFLO performs with accuracy similar to MM5, a fully physical, three-dimensional, nonhydrostatic model.
- Differences between modeled and observed wind values do not necessarily indicate error. Modeled values represent conditions over a smoothly varying surface, whereas observations indicate conditions at a point in a rough landscape.
- Comparison plots of modeled and observed winds for all locations in the observation database can be found on the VCIS Web site at http://www.fs.fed.us/pnw/fera/vent/verification/verifywind/index.html.
- Merging several subdomains generated a nationally consistent database of wind.

Mixing Height

Because the NCEP reanalysis data are at a relatively coarse vertical resolution, they cannot be used to accurately determine mixing heights. Therefore, mixing heights are determined from radiosonde observation (RAOB) data. To derive mixing heights, we lift a parcel of air adiabatically from the surface with a starting temperature near the maximum or minimum daily temperature as described in Holzworth (1972) without adjusting for urban heat effects. The mixing height is that level where the temperature of the adiabatically lifted parcel becomes less than the measured ambient temperature. Once this occurs, it is assumed that the parcel, being cooler than its surroundings, will reach neutral buoyancy and stop rising.

The calculated mixing heights are interpolated between RAOB sites (fig. 5) by using the Cressman scheme (1959) as described in Manning and Haagenson (1992). Frontal boundaries between air masses are not considered, partly because they are difficult to determine automatically from archived data, and also because we assume that their exact position is not critical in a climatological assessment of mixing height. Thus mixing height is mapped to smoothly vary over the landscape except on calm, clear nights when the morning mixing height is modified by local inversions (see “Local Inversion Potential”) and where interpolated mixing heights intersect higher terrain (see “Adjusted Mixing Height”).

Mixing Height Verification

We used a standard method of deriving mixing height and verified our methods against mixing heights derived by the EPA (US EPA 2001) for the years 1984 to 1990. At each radiosonde location, we created scatter diagrams of mixing heights to help

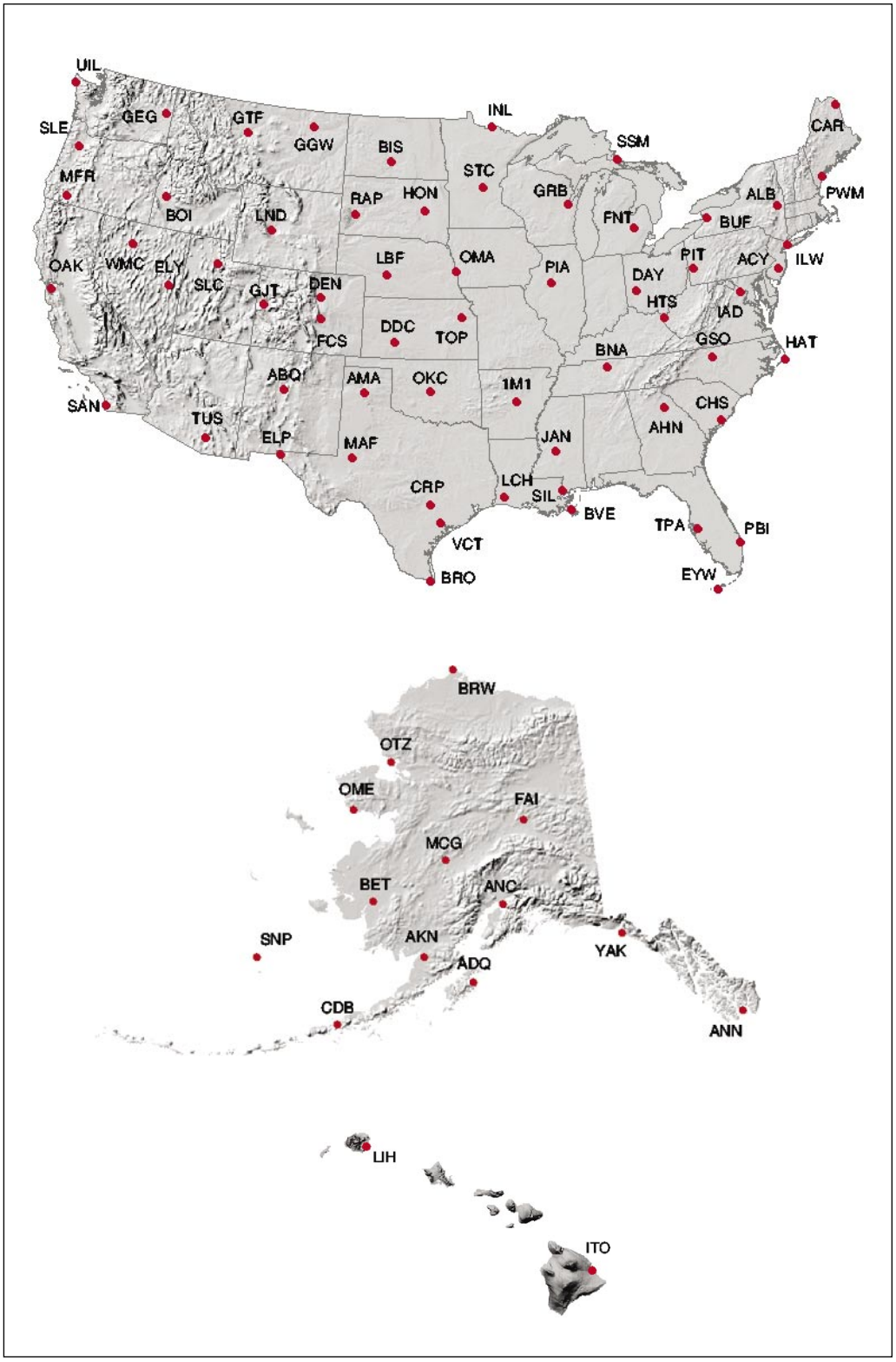

Figure 5—Available radiosonde locations used to calculate mixing height in the contiguous 48 states, Alaska, and Hawaii.

highlight differences. Figure 6a shows an example from Pittsburgh, Pennsylvania. Points falling on the diagonal indicate perfect agreement. Most values agree quite well. Significant differences arise for the treatment of missing data (solid blue triangles); our missing values were omitted, but EPA missing values were filled with interpolated values. Differences also occur for temperature change values (open green triangles). The EPA adjusted values when the selected temperature values were less than the 1200 UTC RAOB temperature, but we made no adjustments.

Two sites, Omaha, Nebraska, and Corpus Christi, Texas, show significant differences in all values (fig. 6b, 6c). We are investigating the cause of these discrepancies. Until we isolate and fix the cause, mixing-height values in regions around these sites should be used cautiously.

Local Inversion Potential

At night, in addition to the effects of stable air and lower mixing height, downslope winds and terrain features contribute to cooling air being trapped in stagnant pools forming patterns of local temperature inversions in places poorly represented by RAOBs. These areas also can trap smoke and other pollutants. Currently there is no meteorological model that can adequately simulate the timing and location of local inversions on a national scale. Therefore, we created a set of algorithms that determine the occurrence, location, and strength of local temperature inversions based on climate records of nearby surface weather stations and terrain features.

Local inversion occurrence—To determine the occurrence potential of a local inversion, criteria were adapted from Pasquill (1962) and Turner (1964) who describe the formation of a surface-based temperature inversion as dependent on surface windspeed and net long-wave radiation leaving the lowest layer of the atmosphere, which depends on cloud cover. Hourly values of windspeed, total cloud cover, opaque cloud cover, and present weather (defined as fog, drizzle, rain, snow, etc.) (National Climatic Data Center 1997, National Renewable Energy Laboratory 1992) are used to determine whether a stable surface layer will form. The potential for a local inversion to occur begins if the following criteria are met for at least 50 percent of all reported hours between 1800 and 0600 local time:

- Windspeed is ≤3 m/s, total cloud cover is ≤80 percent of total sky, and opaque cloud cover is ≤60 percent of total sky; or
- Windspeed is >3 m/s but ≤5 m/s, the total cloud cover is ≤60 percent and opaque cloud cover is ≤30 percent; or
- If fog has been reported at any hour between 1800 and 0600 local time.

On nights with excessive missing data, no inversion is expected if there are more than two reports of winds exceeding 5 m/s. If all reported winds are less than 5 m/s, then the available hours of cloud cover are used to determine inversion potential.

Criteria for the occurrence of a local inversion were checked at all available surface stations, then applied to grid cells in the surrounding neighborhood (fig. 7). If a surface-based inversion were determined to occur at the observing station, then all grid cells within the neighborhood also were assumed to have a local inversion potential. Figure 7 shows how neighborhoods are spaced in the contiguous 48 states and Alaska. Local inversion potential was not determined in Hawaii because the 2.5-minute latitude-longitude grid resolution could not resolve island valleys.

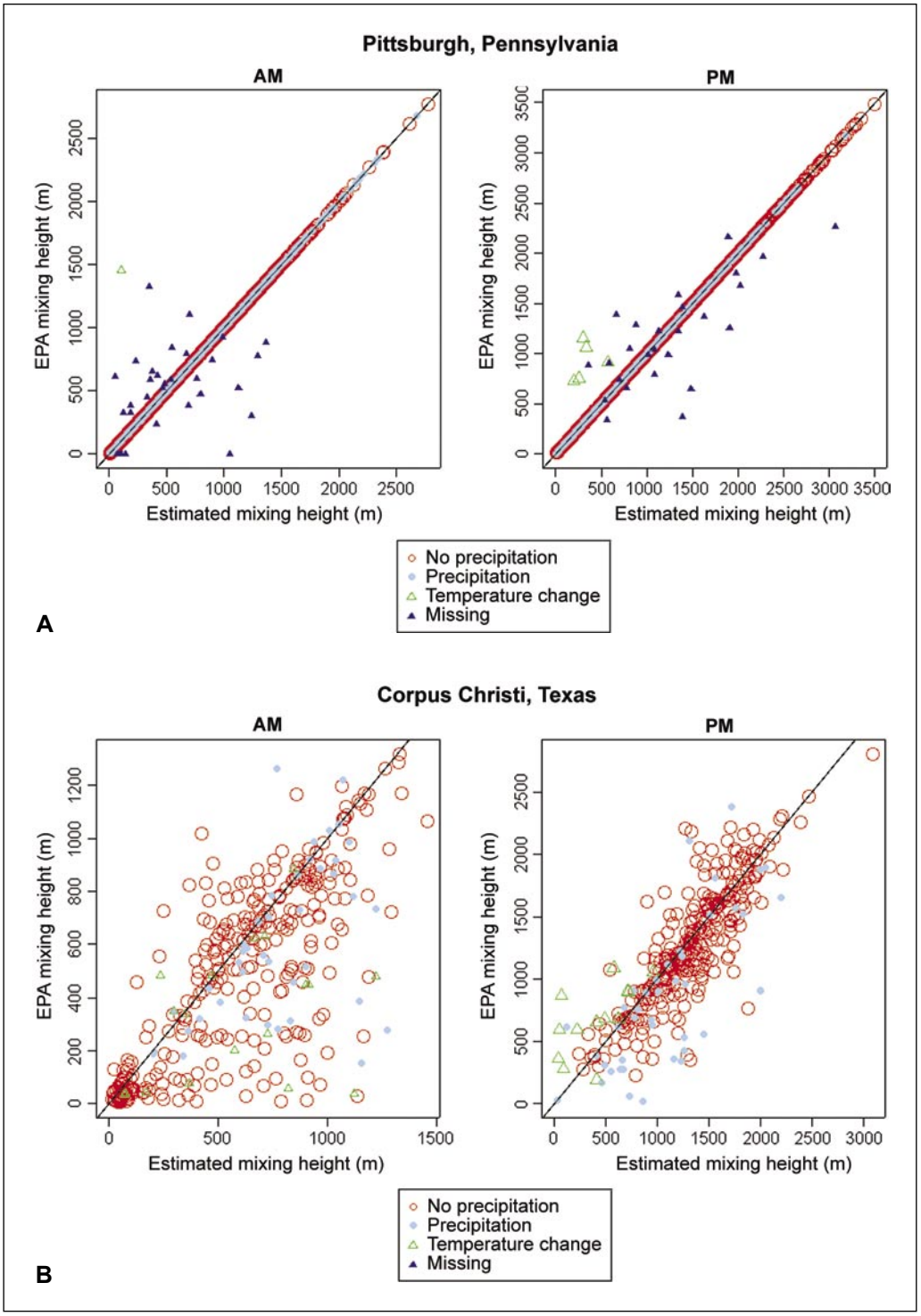

Figure 6—Mixing heights calculated by U.S. Environmental Protection Agency (EPA) versus ventilation climate information system data for morning (AM) and afternoon (PM) at (A) Pittsburgh, Pennsylvania, (B) Corpus Christi, Texas, and (C) Omaha, Nebraska. Only data that differ by more than 5 meters are shown. Values are shown for days with no precipitation (open red circles), with precipitation (solid blue circles), when a temperature change occurred (open green triangle), and when missing data were estimated in the EPA algorithm (solid blue triangles).

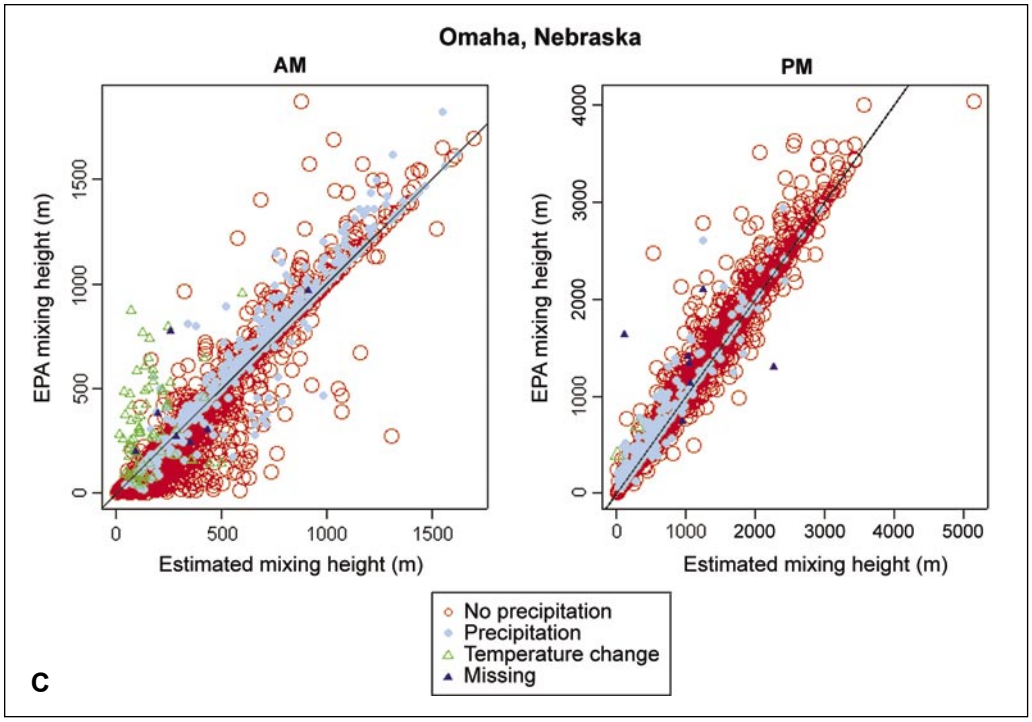

Figure 6—Continued.

Local inversion location—To locate and rank potential local inversions, a GIS algorithm was developed to identify terrain features that promote the collection and trapping of subsiding air, following initial suggestions from Dr. Jan Henderson.[4] An area centered over the intermountain region of the United States is used as an example of how local inversion potential is determined on a 5-km modeling grid with the following steps:

1. Height is vertically exaggerated by five times (fig. 8). This helps to highlight shallow valleys and hollows that are difficult to resolve with 5-km grid cells (pixels).
2. Flat areas are defined by slope that is less than 0.8 degrees and, to eliminate insignificant flat areas, a 3- by 3-pixel smoothing filter is applied (fig. 9).
3. Valleys and basins are defined by negative curvature, which is smoothed with a one-cell radial filter (fig. 10).
4. Flow accumulation is computed for areas exceeding 17 pixels (fig. 11). The 17-pixel threshold is chosen subjectively to eliminate flow potential that crosses ridgelines or begins at mountaintops. With a 5-km grid size, the threshold is 425 km^2.
5. Because not all places of negative curvature (e.g., benches) will form a local inversion, potential areas of pooling are defined by places where lines of flow accumulation intersect valleys and basins.

[4]Henderson, J. 1998. Personal communication. Ecologist, USDA Forest Service, Pacific Northwest Region, Mount Baker-Snoqualmie National Forest, 21905 64th Avenue W, Mountlake Terrace, WA 98403.

Figure 7—Neighborhoods for determining local inversion potential in the contiguous 48 states and Alaska. Letters indicate the National Weather Service identifier for the station that was used to determine calm, clear conditions within the neighborhood, and the yellow dot shows its location.

6. Because not all flat places (e.g., plateaus) will form a local inversion, potential areas of pooling are defined by places where lines of flow accumulation intersect flat areas.

The resulting map of potential inversion locations in the example domain is shown in figure 12.

Local inversion strength—We derived values of strength to help us map inversion heights by assuming that the potential strength of local inversions is correlated to the amount of accumulated flow, which is based on terrain. In general, as flow accumulation increases downstream, so does the inversion strength. Strength values increase rapidly where streams join and when flow is contributed from different airsheds. By

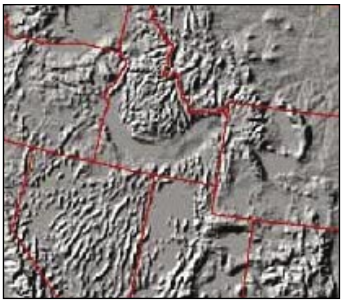

Figure 8—Domain over the intermountain region of the United States with height exaggerated by five times.

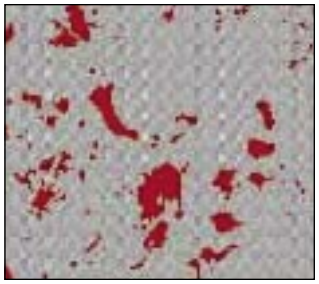

Figure 9—Slope less than 0.8° after 3- by 3-pixel (15- by 15-km) smoothing filter, on the intermountain domain of the United States.

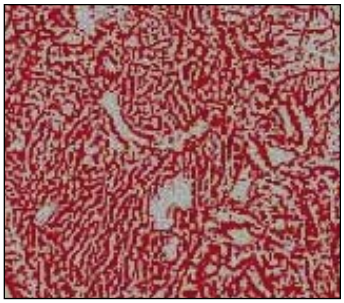

Figure 10—Negative curvature after one-cell radial filter, on the intermountain domain of the United States.

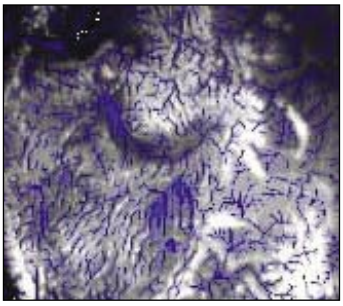

Figure 11—Flow accumulation from at least 17 (15- by 15-km) pixels, on the intermountain domain of the United States.

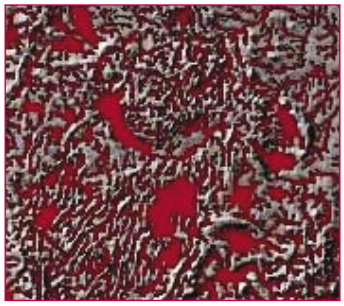

Figure 12—Inversion on the intermountain domain of the United States.

superimposing flow accumulation on the inversion potential map, we derived inversion strength values that ranged from 0 to 11,589, with over 95 percent of the grid cells having a value less than or equal to 366.

To determine the height above ground, we applied a logarithmic function:

$$H = 25.2430 \times \ln\left[S_t \times 1.0404\right] ,$$

where H is the inversion height (m agl) and S_t is the inversion strength truncated at 366. By bounding the inversion strength values at 366 (i.e., all values above 366 were given a value of 366) we keep the inversion height from exceeding 150 m agl, the typical height of nighttime surface-based inversions.[5] Figure 13 shows the resulting inversion locations and relative depths for the 48 states.

Most of the major valleys have inversion strengths less than 366. For example, the Bitterroot Valley in Montana has an inversion strength of about 40, giving it an inversion height of 94 m agl at the valley bottom. The Snake River Valley in Idaho and the mouth of the Columbia River in Oregon have inversion strengths of about 618 and 7,000, respectively. Because both are greater than 366, their potential inversion height

[5] Holzworth and Fisher (1979) found that nearly all surface-based inversions were at least 100 m deep.

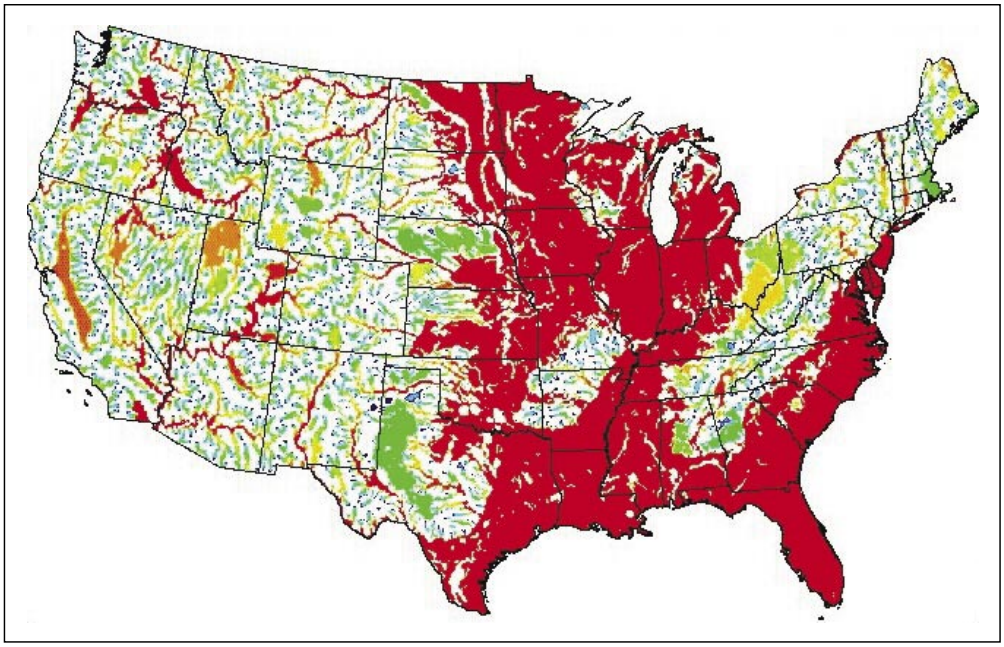

Figure 13—Inversion location and relative depth with red colors indicating maximum flow accumulation depths near 150 m agl and blue colors with minimum flow accumulation. White indicates places where terrain configurations are not expected to influence the formation of local inversions.

at valley bottom is 150 m agl. Note that inversion heights decrease toward the head of the valley. This allows a somewhat smooth transition between areas with a local inversion and areas without a local inversion.

Local Inversion Verification

There are few direct observations of local inversion occurrence or location. At RAOB locations, where surface-based inversions can be directly measured, we tested our inversion occurrence criteria and found that observed surface-based inversions occurred on nearly all days that the criteria of calm wind and clear skies were met. A surface-based inversion was determined to exist if the 1200 UTC RAOB included two adjacent layers within 1000 m of the surface that reported warmer air over cooler air. No distinction was made between inversion strength or depth. The resolution of the temperature data is to the nearest tenth of a degree centigrade.

Table 4 shows “p values” associated with chi-squared tests for each month. A p value less than 0.05 indicates a strong relationship or agreement between the RAOB observed inversion and the surface-based algorithm.

Unfortunately, RAOBs are sparsely distributed over the United States. Additionally, these stations are typically located in flat areas or broad valleys where local inversions are less significant than in narrow valleys, small hollows, and basins that are typical of wildland areas. Therefore, most of our verification techniques for local inversion potential are qualitative in nature.

Figure 14 shows local inversion potential compared to measurements from the Atmospheric Studies in Complex Terrain (ASCOT) experiments in western Colorado (Neff and King 1989). The solid red lines mark elevations at the height of an observed inversion. Gray shades indicate potential inversion derived from terrain features.

Table 4—Comparison between observed inversions from radiosonde observations (RAOB) and predicted inversions from nighttime surface weather

RAOB site[a]	January	February	March	April	May	June	July	August	September	October	November	December
ABQ	0.130	0.060	0.012*	0.026*	0.097	0.084	0.158	0.066	0.012*	0.005**	0.016*	0.018*
ALB	.101	.033*	.011*	.056	.225	.403	.442	.066	.011*	.032*	.035*	.190
AHN	.008**	.018*	.003**	.013*	.004**	.015*	.057	.015*	.004**	.003**	.006**	.008**
BIS	.014*	.013*	.021*	.007**	.020*	.042*	.009**	.043*	.005**	.007**	.011*	.009**
BRO	.040*	.006**	.002**	.009**	.011*	.008**	.038*	.043*	.009**	.007**	.014*	.008**
CAR	.132	.114	.101	.127	.381	.372	.257	.076	.061	.066	.101	.215
DAY	.068	.029*	.015*	.018*	.012*	.024*	.020*	.012*	.002**	.002**	.014*	.174
DDC	.205	.059	.029*	.064	.026*	.074	.222	.205	.010*	.023*	.011*	.205
ELP	.016*	.063	.017*	.020*	.032*	.155	.061	.024*	.032*	.041*	.007**	.007**
ELY	.268	.370	.104	.086	.103	.163	.433	1.000	.251	.272	.107	.130
FNT	.141	.022*	.034*	.021*	.025*	.021*	.045*	.006**	.003**	.009**	.018*	.069
GEG	.169	.088	.020*	.008**	.007**	.009**	.012*	.006**	.007**	.013*	.080	.082
GGW	.101	.041*	.049*	.049*	.029*	.104	.083	.172	.080	.009**	.043*	.046*
GJT	.072	.174	.113	.080	.113	.184	.190	.360	.141	.049*	.184	.138
GTF	.548	.545	.154	.071	.203	.193	.148	.148	.020*	.145	.553	.548
GRB	.064	.011*	.019*	.021*	.008**	.021*	.017*	.009**	.005**	.008**	.012*	.078
GSO	.017	.006**	.002**	.019*	.029*	.010*	.008**	.021*	.004**	.006**	.009**	.021*
HTS	.014*	.037*	.007**	.023*	.021*	.020*	.061	.024*	.029*	.023*	.008**	.020*
IAD	.032*	.018*	.018*	.019*	.033*	.135	.031*	.046*	.009**	.011*	.017*	.020*
INL	.005**	.006**	.002**	.011*	.007**	.021*	.011*	.017*	.006**	.008**	.009**	.018*
LBF	.014*	.013*	.007**	.003**	.011*	.010*	.094	.031*	.014*	.004**	.004**	.002**
LND	.031*	.054	.011*	.015*	.035*	.056	.272*	.241*	.009**	.008**	.047*	.027*
MAF	.035*	.020*	.043*	.049*	.020*	.109	.050	.018*	.008**	.001**	.006**	.006**
MFR	.100	.020*	.011*	.007**	.006**	.001**	.020*	.002**	.006**	.001**	.102	.019*
PIA	.046*	.103	.035*	.042*	.017*	.014*	.068	.038*	.012*	.014*	.017*	.011*
PIT	.068	.060	.006**	.007**	.024*	.057	.020*	.017*	.010*	.007**	.012*	.022*
PWM	.053	.047*	.029*	.027*	.139	.466	.269	.074	.007**	.014*	.032*	.036*
RAP	.017*	.008**	.001**	.003**	.024*	.083	.137	.047*	.004**	.011*	.004**	.015*
SLC	.049*	.107	.047*	.049*	.024*	.042*	.037*	.083	.009**	.059	.024*	.020*
SLE	.080	.011*	.005**	.003**	.008**	.002**	.006**	.002**	.020*	.005**	.045*	.007**
STC	.029*	.240	.050	.026*	.008**	.103	.092	.038*	.016*	.009**	.007**	.021*
TOP	.060	.018*	.008**	.007**	.007**	.026*	.052	.017*	.007**	.001**	.002**	.003**
TUS	.042*	.058	.019*	.031*	.113	.159	.141	.113	.287	.159	.128	.087
UIL	.064	.029*	.006**	.004**	.004**	.004**	.001**	.007**	.002**	.003**	.035*	.031*
WMC	.042*	.165	.031*	.031*	.061	.126	.147	.406	.094	.043*	.030*	.083
YAK	.142	.075	.030*	.029*	.061	.042*	.037*	.023*	.071	.066	.066	.068

"P" scores associated with chi-squared tests are shown for each observation location and each month. * = significant relationship ($p < 0.05$), ** = highly significant relationship ($p < 0.01$).

[a] Row headings represent RAOB site names whose locations can be found in figure 5.

Another way to check the reasonableness of the terrain algorithm is to compare maps of local inversion potential with satellite observations. Figure 15a shows a Moderate Resolution Imaging Spectrometer (MODIS) satellite image over the Salmon River in central Idaho during the 2000 wildfires; a map of local inversion potential for the same general area is shown in figure 15b. Inversion potential is shaded with light blue being the strongest potential. From the satellite image, it appears that most smoke is concentrated in the Salmon River valley, where the strongest inversion potential is indicated. Darker blue colors indicate potential inversions in side valley and tributaries, just as they appear in the satellite image.

Adjusted Mixing Height

The local inversion algorithm was applied only to morning (1200 UTC) mixing heights and only to grid cells in the neighborhood of a surface observation showing calm winds and clear skies the previous night. Grid cells not in a terrain feature that fosters the development of a local, nighttime inversion (i.e., peaks, ridges, plateaus, etc.) are assumed to be experiencing the ambient condition of mixing heights interpolated from RAOB measurements.

Figure 16 shows how mixing height patterns change on a July morning when the local inversion potential is imposed. Note that valley inversions become visible in the Northwestern United States and in the Appalachian Mountains after the inversion algorithm is imposed.

There are times when the measured mixing height passes below ground level as it is interpolated across the landscape. This happens frequently when the mixing height is relatively low, such as during a winter morning, or in places where mountains are between RAOB locations. At these times and in these places, where terrain is above the interpolated mixing height, air parcels often are free to lift to great heights, occasionally reaching the tropopause.[6] Although RAOB measurements can help locate the height of parcel trajectories above the mixed layer, computations were too cumbersome to use in this application. Therefore, we arbitrarily assigned a mixing height, or "free" height, to places where the interpolated mixing height values were at or below ground level. In the afternoon, we set the "free" height to be 4000 m agl, which is about the highest measured afternoon mixing height, and the morning "free" height is set at 1000 m agl, which is about the highest measured morning mixing height (Holzworth 1972). The best way to view the effect of this imposed "free" height is to view time-series statistics of mixing height at individual points, which are available whenever the "Get Stats" button is selected from a domain in the "Maps and Graphs" section of the VCIS Web site (http://www.fs.fed.us/pnw/fera/vent/data.html). The time series are designed as box plots so the user can determine how common a certain mixing height may be at any selected point. Each box plot includes a red line at the imposed "free" height level to help determine the frequency of times that observed mixing heights were mapped below terrain at any point on the landscape. Appendix 2 provides examples and describes how to interpret time-series box plots for VCIS mixing height.

[6] The tropopause marks the boundary between the troposphere, where temperature generally decreases with height, and the stratosphere, where temperature generally increases with height. The tropopause is about 7000 m asl in the polar regions, about 10 000 m asl in the midlatitudes, and about 17 000 m asl in the tropics.

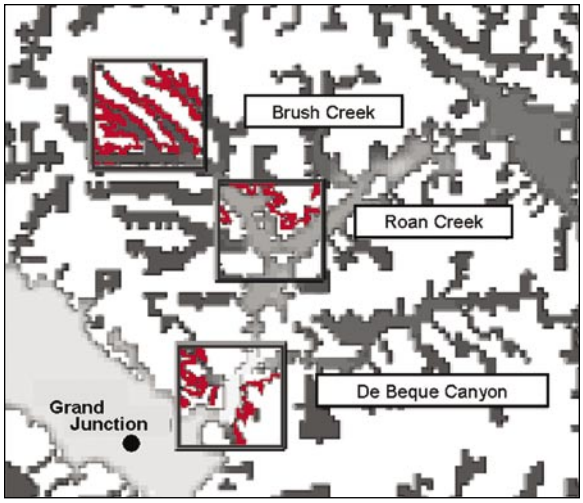

Figure 14—Local inversion potential locations (gray shades) shown with inversion height observations (red lines) in western Colorado.

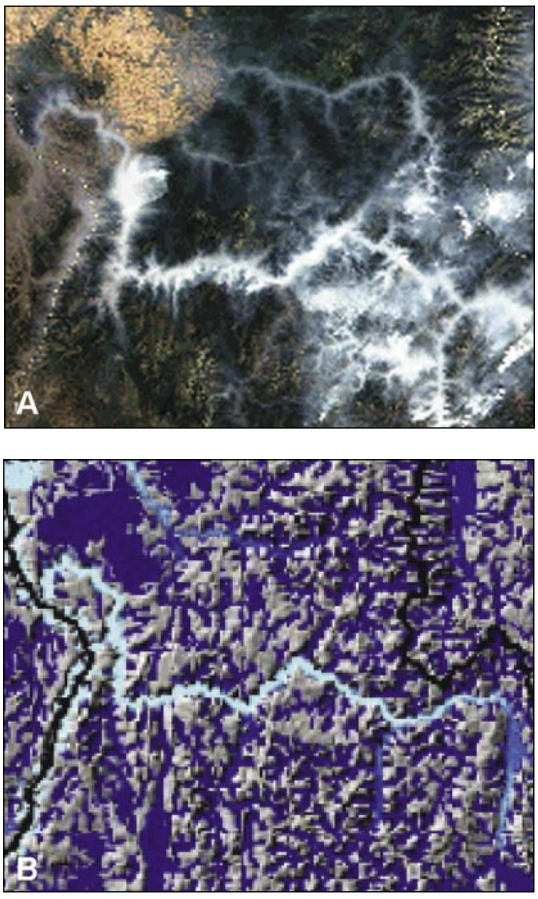

Figure 15—(A) Observations of smoke over central Idaho at about 10 a.m. in July 2000. (B) Map of inversion potential with light blue showing strongest potential and dark blue showing weaker potential.

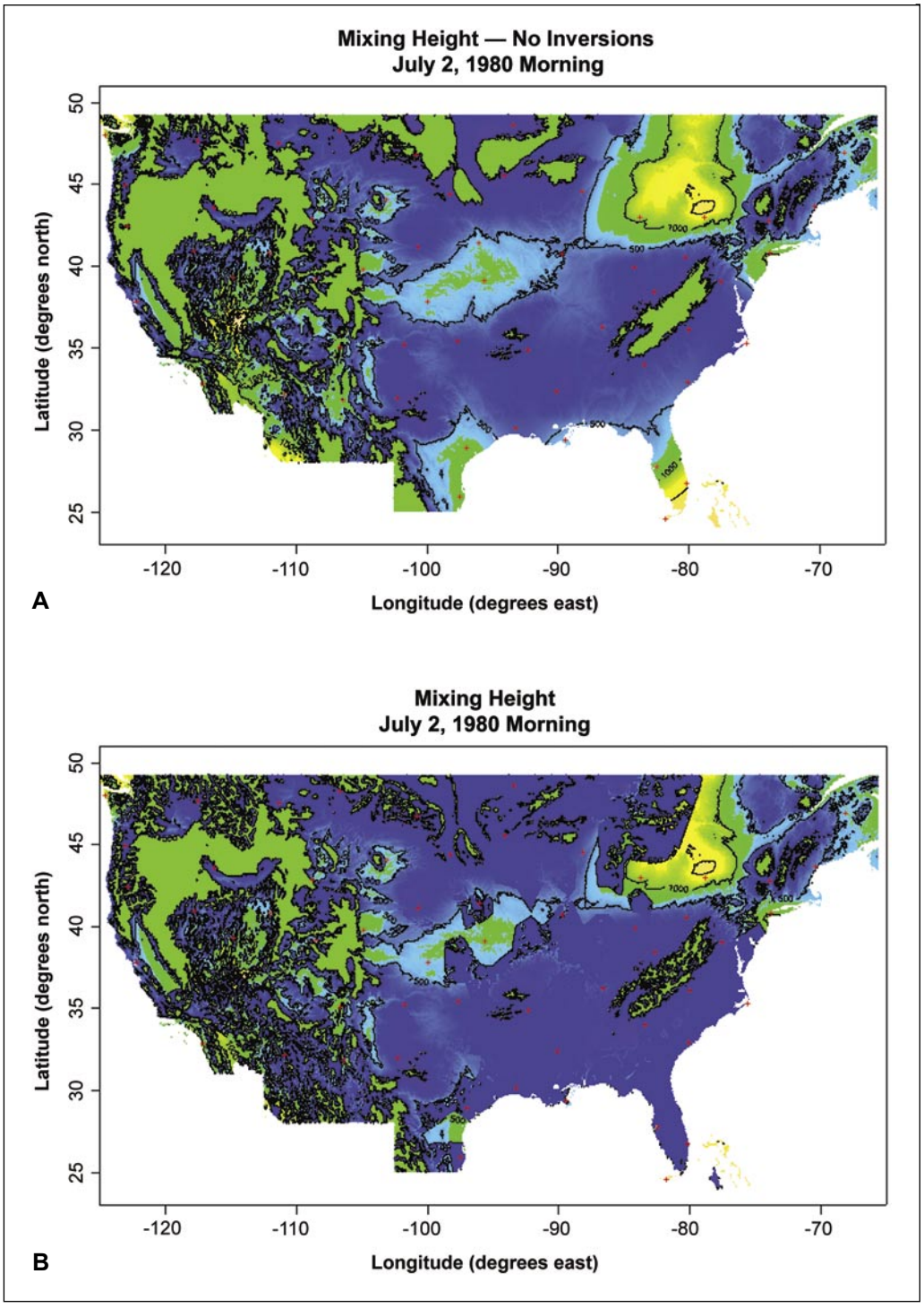

Figure 16—Interpolated mixing height for the morning of July 2, 1980, (A) without adjustment for local inversion and (B) with local inversions. Blue indicates lowest heights, and yellow indicates highest heights.

Figure 17 shows the effect of adjusted mixing heights. In 17a, the observed mixing height is mapped below ground level. Whereas parcels of air at points *a*, *e*, and *g* ventilate in response to the observed mixing height, parcels originating from places above this layer will ventilate higher into the atmosphere. Air parcels originating in basins or valleys that exhibit a potential for local inversion, such as at points *c* and *f*, will be trapped to elevations below 150 m agl. In 17b, the observed mixing height is mapped above ground level everywhere. The ventilation of air parcels originating from anywhere except in places with local inversions (points *c* and *f*) will respond to the height of the observed mixing layer. In this case, smoke plumes originating from points *a*, *e*, and *g* may loft to higher elevations than in 17a when observed mixing heights are lower. But plumes originating from points *b* and *d* may not be ventilated as well as in A because in B these points are below the observed mixing height, and thus plumes do not lift to the "free" height.

Note that, in reality, the tropopause or an inversion layer in the upper atmosphere that limits mixing will be nearly horizontal relative to sea level but may bend gradually over higher terrain, such as the Rocky Mountains. Although it is somewhat unrealistic to force the "free" height to follow terrain heights, it appears to be an adequate approximation. Also, fixing a height above ground level was the most computationally efficient way to create a positive mixing height value and does not seem to seriously compromise the physical reasonableness of resulting mixing height patterns. Clearly, more rigorous methods of deriving "free" heights are needed.

Also, it should be noted that during winter, patterns illustrated in figure 17a are common where observed mixing heights are somewhat low and map below high terrain, whereas in summer, patterns illustrated in figure 17b are common where observed mixing heights are relatively high and map to elevations just above high terrain. This affects the seasonal distribution of mixing height values in high terrain, causing winter mixing heights to appear higher than summer mixing heights. Although seemingly contrary to intuition, it is not unreasonable.

Key Elements of Mixing Height

- Mixing heights were calculated from RAOB measurements by using a standard parcel method.
- Values of mixing height are generally consistent with EPA-derived values.
- When observed mixing heights are mapped at or below ground level, an arbitrary height of 4000 m agl in the afternoon or 1000 m agl in the morning is imposed. This may cause mixing heights at high-elevation locations to be higher during winter than summer at times.
- Morning mixing heights are adjusted to account for local, surface-based inversions that are common in valleys and basins at night.
- Surface observations of wind and cloud cover can correctly predict the occurrence of a local, surface-based inversion most of the time.
- Local inversion potential is applied only to grid cells in the neighborhood of a surface observation site showing calm, clear conditions at night.
- An algorithm based on terrain features can correctly predict the location of a local inversion most of the time.

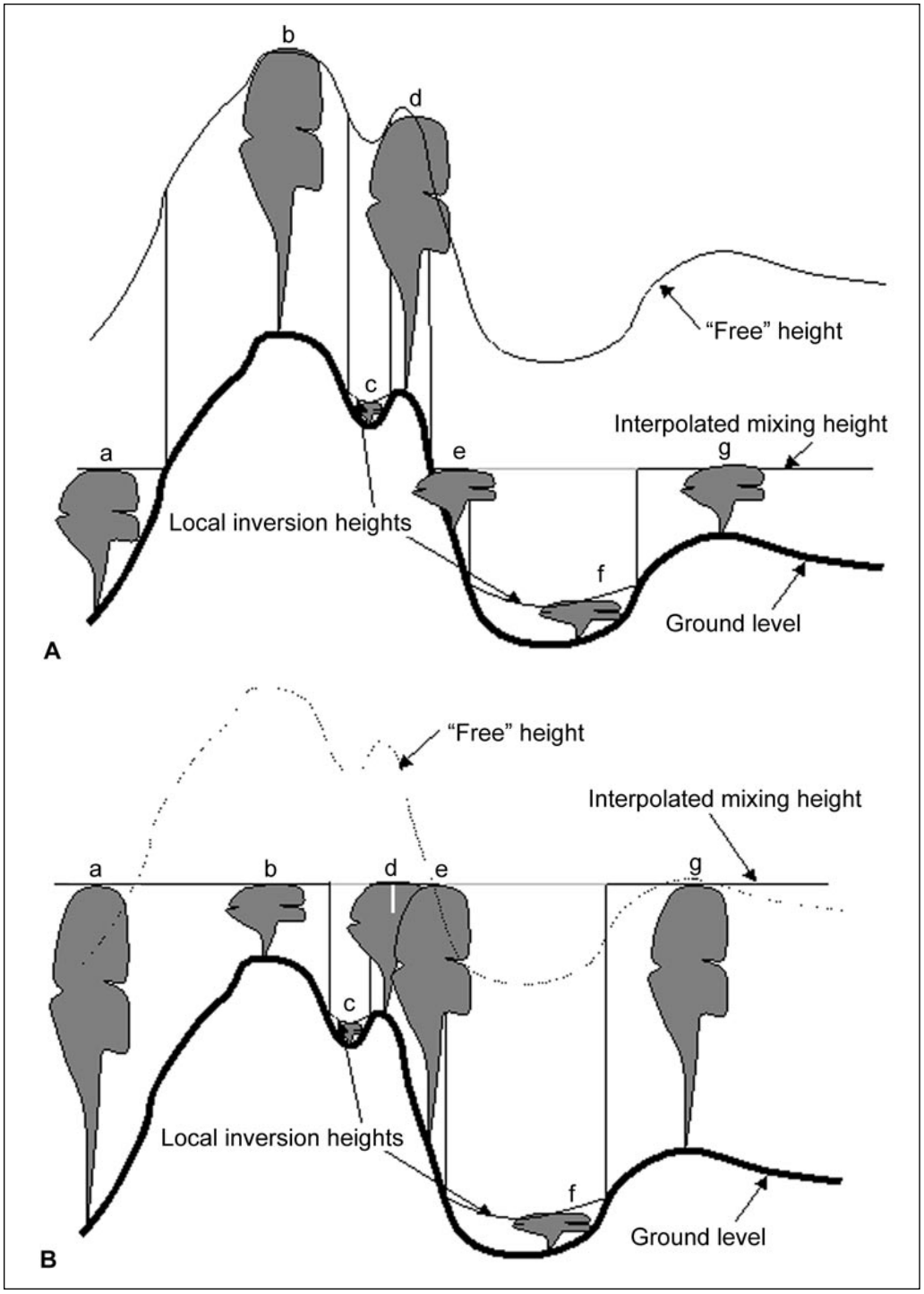

Figure 17—Schematic diagram of adjustments to the mixing height in areas of complex terrain. The observed mixing height is interpolated between radiosonde observation measurements; local inversion heights are determined by the amount of downslope flow accumulation and invoked only on mornings following calm, clear nights; the "free" height is arbitrarily set at 4000 m agl during the afternoon and 1000 m agl in the morning. Gray clouds indicate potential vertical mixing for (A) when interpolated mixing height maps below ground level in places, and (B) when interpolated mixing height maps above ground level. Ground level is the heavy black line.

Click here for Part 2

Click here to return to Part 1

- Local inversion potential is applied only to grid cells within terrain features that foster the formation of the development of a nighttime inversion. The height of a local inversion is capped at 150 m agl and determined by the amount of potentially accumulating nighttime drainage flow.
- Discontinuities in mapped values of morning mixing height occur when adjacent surface observation stations experience different nighttime conditions, causing the local inversion algorithm to be invoked in one neighborhood and not in the other.

Ventilation Index

The ventilation index has become a useful tool for air pollution management throughout the United States. Fire and smoke managers in the Southeastern United States are most familiar with using a ventilation index, and several states use the index, sometimes called a clearing index, to help regulate outdoor burning (Hardy et al. 2001). Although popular as an assessment and prediction tool, until now there has been no historical review of ventilation potential. This has prevented an understanding of the spatial and temporal variability of ventilation and its associated impact on values of air quality and visibility.

The ventilation index is the product of windspeed and mixing height. Usually, the index is derived from the average value of windspeed in the mixed layer or a local steering wind, which often is well above 10 m, the height of wind derived for this study. Also, we have modified the mixing height to account for local inversions. The local inversion correction creates lower values of ventilation potential at remote sites, which are more applicable than indexes calculated from a central RAOB location. Therefore, values of ventilation index in VCIS are relatively conservative and may best be applied to smoke concerns relatively close to the ground.

To map index values in a meaningful way and help assess the values of air quality and visibility that are at risk from wildland fire, we followed a common procedure of classifying the ventilation index into categories of poor, marginal, fair, and good. We assigned a classification scheme with ventilation index values that are half the values of commonly used classes (Hardy et al. 2001), however, because windspeeds at 10 m agl typically are about half of those at 40 m agl, which is closer to the height of a trajectory wind. The resulting classification scheme is summarized in table 5.

Figure 18 illustrates the monthly mean classifications of ventilation index for October in the contiguous 48 states. Note the large areas of relatively poor ventilation potential in low-lying areas during the morning. During the afternoon, the ventilation potential improves dramatically. Marginal conditions prevail, however, in the lee of several mountain ranges. Monthly mean maps of the ventilation index classes are available on the VCIS Web site (http://www.fs.fed.us/pnw/fera/vent/data.html) for all months and all 50 states. The interactive Web site allows users to plot sensitive receptors, such as hospitals, schools, airports, wilderness areas, and highways as overlays on the ventilation index maps. In addition, users can zoom, pan, add elevation contours, cities, state and county boundaries, and rivers and railroads to help exactly locate areas of potentially high risk.

In addition to maps of ventilation index classifications, the temporal variability of ventilation indexes can be viewed from the VCIS Web site for any point on the landscape through frequency plots of all twice-daily values. The frequencies are shown as box plots, making it possible for users to determine the chance of experiencing a desired ventilation index value on any day of the month. Also available are plots that show the

Table 5—Classification of ventilation potential from ventilation index values in the ventilation climate information system database

Ventilation index	Classification
Square meters per second	
0–1175	Poor
1176–2350	Marginal
2351–3525	Fair
>3525	Good

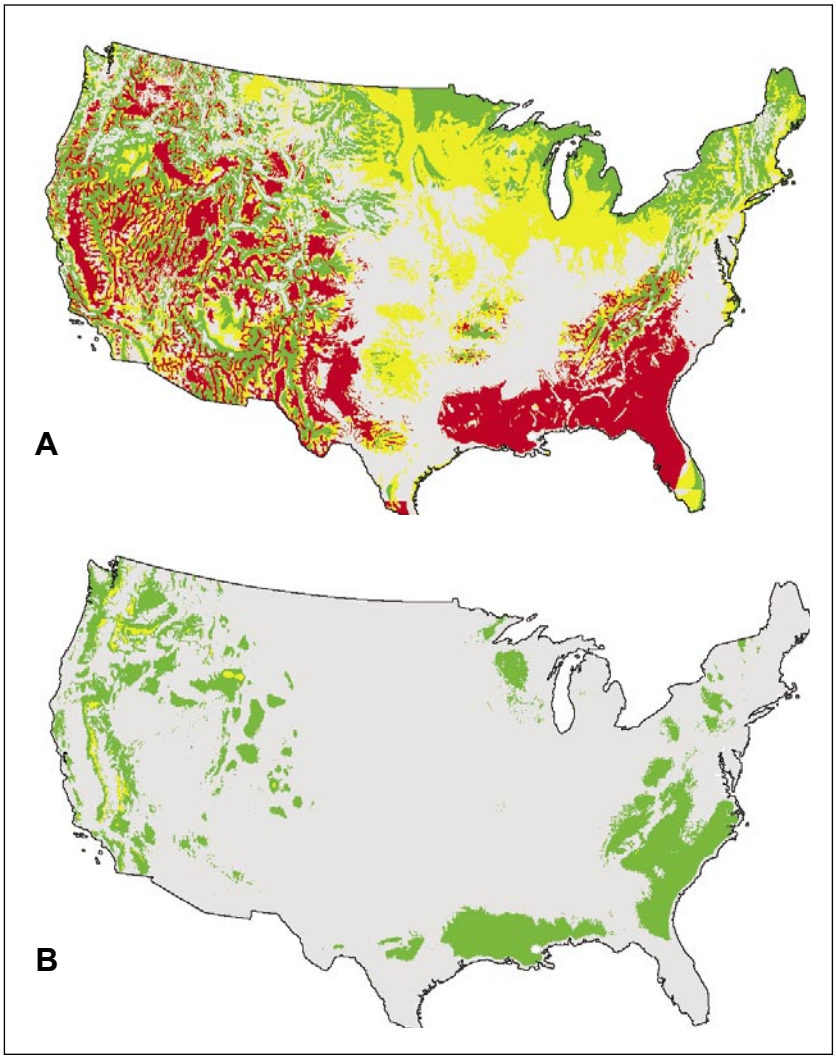

Figure 18—Monthly mean maps of ventilation index classifications for (A) morning and (B) afternoon in October. Red represents potentially poor ventilation conditions, yellow is marginal, green is fair, and gray is good.

year-to-year variability of values for each month. In these plots, the index is not limited to classes, but the full range of actual values can be viewed. Appendix 2 provides examples and explains how to interpret the box-plot time series of ventilation index.

Ventilation Index Verification

As an index, one only can judge its value from its measured components, which are windspeed and mixing height. Modeled winds were shown to be reasonably accurate in many cases, with randomly distributed errors within a range of observation accuracy. There seems to be a relatively consistent slow bias, however, mainly during spring and early summer in high desert regions and flat, grassy areas. Mixing heights always appear reasonably accurate, except within tens of kilometers from Omaha, Nebraska, and Corpus Christi, Texas. It is difficult to determine the accuracy of the local inversion potential, however, because there are so few observations. Also, the relatively coarse grid size (2.5-minute latitude-longitude and 5 km) does not capture many of the small hollows that can trap smoke at night. With the somewhat slow windspeed and inclusion of local valley inversions, we assume that the ventilation index errs conservatively, biasing toward potentially poor ventilation. Although there are missing data in the 40-year record, the long time series ensures reliable interpretation of temporal patterns.

Key Elements of Ventilation Index

- The ventilation index derived for VCIS is most useful for addressing concerns about smoke that stays relatively close to the ground.
- The ventilation index is somewhat conservative but provides a reasonably accurate view of ventilation climate during the last 40 years.
- The VCIS provides the first national coverage of ventilation climate.

Risks to Air Quality and Visibility From Wildland Fire

Development of a fine-resolution database of surface winds, mixing height, and ventilation index affords a unique opportunity to assess the risks to air quality and visibility from wildland biomass burning at various scales. Although model-generated data can only approximate actual conditions, the mapped products and point statistics show reasonable patterns of information and provide the most accurate representation of historical ventilation potential to date. Therefore, conclusions should be used cautiously but not without some confidence.

Risks to air quality occur when ventilation index values are low and harmful pollutants are held close to the ground. Risks to visibility also occur when ventilation index values are low. Light-scattering and absorbing elements of smoke near the ground cause significant degradation of visual range, especially when combined with high atmospheric humidity.

Although we base our estimate of risks to air quality and visibility solely on an index of ventilation potential, more precise estimates can be derived by combining ventilation potential with historical smoke emissions and atmospheric humidity data. Because emissions and humidity data currently are unavailable at a consistent temporal and spatial resolution and they are much more difficult to derive than mixing height and wind, they are not included in this assessment. Where available locally, however, they can be used to help refine the risks identified by ventilation index.

Spatial patterns of the monthly mean ventilation index can be viewed on the VCIS Web site (http://www.fs.fed.us/pnw/fera/vent/data.html). In general, ventilation index data show the greatest risks to air quality and visibility in the Southeastern United

States where marginal to fair ventilation conditions prevail most of the year. This region also has a high concentration of roads, hospitals, and schools. Additionally, the northern plains and deep valleys of the Western United States show risk potential with consistently poor to marginal ventilation during winter and marginal to fair conditions during spring and autumn. Sensitive receptors in the northern plains and western valleys, however, are much more sparse than in the Southeastern United States.

Site-specific information on temporal patterns of ventilation indexes can be viewed from the VCIS Web site by selecting the “Get Stats” button in the “Maps and Graphs” section. At each point, periods of good ventilation potential can be found at times throughout the year. Some places have greater frequency of good ventilation and there are some times that are better than others. There also are places and times when poor ventilation conditions prevail.

To help summarize the data, we divided the country into significant airsheds as defined by the United States Geological Survey hydrologic unit code (HUC) system (Seaber et al. 1987) (fig. 19). The contiguous 48 states were divided according to first-order hydrologic units. The second-order hydrologic units were used to represent airsheds in Alaska. Hawaii is considered a single, separate airshed.

The average ventilation index for each regional airshed is shown in table 6. The table is color coded to highlight values that fall into the range of index classifications of poor (0 to 1175 m^2/s), marginal (1176 to 2350 m^2/s), fair (2351 to 3525 m^2/s), and good (>3525 m^2/s) as red, yellow, green, and white, respectively. During morning hours, marginal to fair ventilation conditions prevail throughout most of the country with relatively poor ventilation potential during summer in the Mississippi regions and South-Atlantic Gulf region. Ventilation potential improves for most of the country during the afternoon. The Mississippi regions, other central U.S. regions, and South-Atlantic Gulf region, however, retain marginal to fair ventilation potential during winter.

Ventilation potential is dominated by wind in the morning, but afternoon ventilation is dominated by mixing height. The highest ventilation potential prevails during spring and early summer in the high desert regions of the country where intense heating causes very high mixing heights. These places include the Rio Grande, Upper and Lower Colorado, and Great Basin airsheds, with high indexes extending well into early autumn in the Rio Grande airshed. The Arkansas-White-Red airshed in the south-central states also experiences high ventilation potential during midsummer when afternoon heating is greatest.

Counter to most of the rest of the country, the highest ventilation indexes in the Pacific Northwest occur during winter. Although the Columbia Basin that is centered in the Pacific Northwest region consistently experiences marginal ventilation potential during winter, high mountains that dominate the remainder of the airshed receive their highest winds in winter, and thus high ventilation potential. Also, high terrain in the Pacific Northwest often rises above interpolated mixing height values in winter, causing the 4000 m agl arbitrary level to dominate mixing height values at this time of year. This may create artificially high ventilation potential in this airshed during winter.

Although prevailing ventilation conditions may indicate the likelihood of risk to values of air quality and visibility in each region, in all places at many times of the year good ventilation conditions can occur. The “Get Stats” button from the “Maps and Graphs” page of the VCIS Web site (http://www.fs.fed.us/pnw/fera/vent/data.html) shows the frequency of potentially good ventilation potential on any day of the month or any

Figure 19—Regional airshed boundaries for the contiguous 48 states and Alaska. Hawaii is a single, separate airshed.

month of the year for individual grid points. To illustrate the regional variability of the ventilation index, we created a series of box plots (figs. 23 through 25 in app. 3) that show the median, standard deviation, and range of values for each month. Although the ventilation index ranges from zero to well over 70 000 m^2/s, the box plots are truncated at 14 000 m^2/s in the afternoon and 7000 m^2/s in the morning to better illustrate the range of management categories, where any value above 3525 m^2/s is considered good ventilation potential.

From the box plots (see app. 3), it appears that all areas can experience good ventilation and low risk to values of air quality and visibility at times during the morning (range bars exceed 7000 m^2/s), but the Great Lakes region clearly experiences the best morning ventilation potential within a standard deviation of its median, especially

Table 6—Average ventilation index values for each regional airshed and each month. Red = poor (<1175), yellow = marginal (1176 to 2350), green = fair (2351 to 3525), and white = good (>3525)

Hour	Regional airshed	January	February	March	April	May	June	July	August	September	October	November	December
							Square meters per second						
Contiguous 48 states													
AM	Arkansas-White-Red	1699	1883	2152	2042	1916	1567	1341	1248	1510	1652	1904	1800
	California	2334	2389	2313	2125	2040	1757	1526	1396	1639	1793	2176	2265
	Great Basin	1826	1927	2038	1882	1677	1398	1353	1282	1449	1513	1862	1881
	Great Lakes	3713	3095	3363	3273	2371	2049	1616	1809	2381	3325	4135	3959
	Lower Colorado	2129	2089	2232	2087	1827	1574	1466	1419	1696	1852	2002	2065
	Lower Mississippi	1578	1795	1896	1661	1541	1101	863	795	1122	1252	1787	1762
	Mid Atlantic	2912	2754	2849	2701	2100	1796	1587	1612	1776	2223	2775	2799
	Missouri	2421	2188	2343	2322	2031	1679	1386	1397	1806	2184	2319	2336
	New England	2965	2784	3164	3033	2396	2151	1834	1883	2092	2553	3215	2954
	Ohio	2752	2386	2536	2522	1809	1413	1190	1175	1451	1836	2505	2636
	Pacific Northwest	2818	2726	2495	2249	1979	1809	1638	1569	1839	2181	2770	2769
	Rio Grande	1887	1928	2174	2004	1840	1549	1319	1252	1482	1647	1923	1863
	Souris-Red-Rainy	1926	1815	2130	1940	1804	1617	1199	1341	1892	2483	2228	1890
	South Atlantic Gulf	1525	1742	1749	1576	1336	1215	1115	1070	1210	1244	1493	1506
	Tennessee	2179	2207	2256	2169	1769	1372	1212	1160	1410	1695	2158	2232
	Texas Gulf	1415	1667	1889	1925	2062	1815	1484	1335	1375	1441	1685	1584
	Upper Colorado	1971	1897	2214	2053	1836	1568	1407	1388	1654	1744	2044	2010
	Upper Mississippi	2003	1773	2216	2109	1669	1391	1058	1097	1462	1959	2129	2008
PM	Arkansas-White-Red	3238	3891	5295	6705	6427	6672	8339	7626	6364	4650	3951	3166
	California	5823	5145	4999	5456	5665	5998	5991	5675	5019	4531	5337	6009
	Great Basin	4454	4092	5415	6413	6764	7795	7768	7021	5985	4352	4203	4402
	Great Lakes	3750	3803	4824	6632	6504	6430	5876	5524	5463	5118	4294	3618
	Lower Colorado	3620	4020	6100	7863	8747	9884	8255	6813	6347	4870	3982	3474
	Lower Mississippi	2930	3526	4516	5160	4952	4907	4815	4725	4661	3898	3558	2973
	Mid Atlantic	4200	4218	4796	5523	5275	5176	4805	4338	4064	4070	4144	4332
	Missouri	4771	4288	5006	6964	6573	6497	6609	6213	5498	4921	4588	4649
	New England	4794	4799	5368	5753	5569	5611	5020	4636	4427	4527	5038	4594
	Ohio	3317	3345	4520	5528	5182	4895	4508	4298	4400	3938	3635	3249
	Pacific Northwest	8715	6438	5010	5237	5231	5618	6041	5694	4651	4451	6980	8756
	Rio Grande	4217	5352	7848	9430	10 673	11 132	9795	7755	7121	5629	4645	4293
	Souris-Red-Rainy	2485	2752	3576	6244	6585	6101	5498	5258	4837	4276	2861	2189
	South Atlantic Gulf	2974	3624	4512	5155	4944	4736	4675	4210	4087	3682	3299	2944
	Tennessee	3791	3982	4778	5489	4962	4735	4414	4123	4213	3850	3831	3913
	Texas Gulf	2969	3586	4863	5873	5899	5769	6969	6971	5483	4291	3689	2959
	Upper Colorado	5863	4809	5626	6810	7336	7861	6919	6219	5838	4375	4926	5749
	Upper Mississippi	2426	2500	3817	5563	5614	5171	4540	4235	4238	3806	2910	2300

Table 6—Average ventilation index values for each regional airshed and each month. Red = poor (<1175), yellow = marginal (1176 to 2350), green = fair (2351 to 3525), and white = good (>3525) (continued)

Hour	Regional airshed	January	February	March	April	May	June	July	August	September	October	November	December
							Square meters per second						
Alaska													
AM	Southeast	3650	3489	3217	3106	2321	2075	1768	1933	2388	3139	3350	3370
	South Central	3266	3064	2890	2529	2129	1986	1714	2033	2526	2768	2941	3131
	Southwest	2997	2856	2810	2569	2461	2007	1988	2415	2920	3068	2893	3025
	Yukon	2710	2588	2443	2156	1971	1806	1908	2118	2386	2489	2532	2634
	Northwest	2965	2883	2896	2667	2341	1965	2234	2548	2911	2901	2905	2895
	Arctic Slope	2112	2052	1894	1896	1871	1770	1804	2064	2525	2294	2067	2090
PM	Southeast	12 007	10 413	7558	6272	4888	4519	4255	5081	6586	8789	11 231	12 182
	South Central	13 107	11 981	9159	5820	4337	4100	4113	5173	7032	9760	11 625	13 047
	Southwest	10 218	8132	5302	4373	4607	4226	3750	4092	4782	5432	8596	10 396
	Yukon	11 740	9829	6303	4687	4820	4596	4329	4374	5023	6919	10 599	11 516
	Northwest	13 143	11 747	9846	6997	6145	4908	4469	4517	5114	7685	12 069	12 390
	Arctic Slope	9351	8565	6968	5222	4386	4191	4393	4664	5061	6640	8834	9082
Hawaii													
AM		2310	2223	2847	2964	2884	2932	3148	2930	2660	2642	2648	2391
PM		4341	4179	5183	5248	5025	5034	5276	4980	4645	4681	4977	4382

during winter. The standard deviations of values generally range from poor to fair during the morning in most regions. This suggests that values of air quality and visibility throughout the country are most likely to be affected during the late night and early morning.

The box plots show that most places have significant potential (within a standard deviation of their median) of reaching good ventilation conditions during the afternoon at any time of the year. Exceptions include the Upper and Lower Mississippi regions, which, while exhibiting some good ventilation occurrences at all times of the year, seldom reach fair conditions in winter. Good conditions occur within a standard deviation only in April and May. Thus, it may be more difficult to find good ventilation conditions in the Mississippi regions than elsewhere.

Another note of interest is the large range of ventilation conditions in California. Its box plot shows that the frequency of good conditions is nearly the same as the frequency of very poor conditions, no matter what time of year. Although other regions may confidently expect good ventilation conditions in July, for example, the chances of finding good conditions in the California region are equal to finding poor conditions. This makes seasonal planning in the California region more difficult than for other regions.

The data suggest that all areas experience times of good ventilation. Therefore, it should be possible to mitigate potential impacts on values of air quality and visibility. In some places, however, good ventilation conditions are less frequent than marginal or poor ventilation conditions, and in most places good ventilation is infrequent during morning hours. At these times and places, balancing the risk to air quality and visibility with other management objectives may be challenging. The data show highly variable conditions, however, in both space and time. The VCIS, which illustrates the frequency and spatial distribution of ventilation conditions that may impact values of air quality and visibility, may help quantify potential risks.

Key Elements of Risks to Air Quality and Visibility From Wildland Fire

- Risks to air quality and visibility from wildland fire can be estimated by assessing spatial and temporal patterns of ventilation index.
- The greatest risks to air quality and visibility from wildland fire occur in the Southeastern United States.
- Risks to air quality and visibility from wildland prescribed fire can be minimized by planning times when good ventilation conditions are most frequent.
- The best ventilation conditions during morning hours occur during winter along the northern coasts of the contiguous 48 states, in southern Alaska, and in the north-central plains.
- The best ventilation conditions during afternoon hours occur in spring and early summer in the Rio Grande airshed.
- The VCIS point statistics allow identification of times of highest or lowest risk at any point on the landscape.
- The VCIS monthly maps show the spatial patterns of potential risk.

Conclusions

The VCIS assists users in assessing values of air quality and visibility at risk from wildland fire by illustrating the spatial and temporal variability of ventilation potential. The 40-year, twice-daily time series at 2.5-minute latitude-longitude and 5-km spatial resolution can be viewed as monthly averaged maps of index classifications or in plots of frequency and magnitude at selected points. The ArcIMS Web-access system allows users to view local to national patterns of ventilation potential. Overlays of sensitive receptors (hospitals, schools, roads, airports, etc.) can help quantify the proximity of risk to poor ventilation conditions.

Creation of such a high-resolution climate information system, with over 100 gigabytes of data, was only possible with high-level computing power. Even so, the amount of smoothing and simplifying assumptions needed to process the data in a reasonable amount of time could be reduced with even more computational energy. Also, whereas the long climate record may compensate for missing data, increased computer resources could reduce the number of missing values in wind by allowing numerical calculations to continue longer before reaching a stable solution and in other variables by using additional algorithms to fill missing data. Nevertheless, the generated values provide a reasonably accurate view of ventilation potential and associated risks to air quality and visibility in the United States. The products include several unique features:

- The first nationally consistent, historical database of surface wind at fine spatial resolution.
- The longest historical record and finest spatial resolution of mixing height.
- The first database of historical ventilation potential.
- The first physically reasonable assessment of historical risks to air quality and visibility.

Because the VCIS offers the first historical perspective of ventilation potential and associated risks to air quality and visibility at a high spatial and temporal resolution on a national scale, the information it holds about patterns and probabilities of risk is just beginning to be explored. As users are being introduced to the products, however, several applications to land management emerge. These include:

- Identification of areas at risk to smoke problems
- Smoke management planning
- Airshed assessments
- Better understanding of the spatial and temporal variability of atmospheric conditions that affect smoke dispersion

Although we adopted a relatively simple approach to assessing values at risk, it was not a trivial task to create the necessary products for analysis. As use increases, however, it may become beneficial to add detail and increase accuracy. For example, the 2.5-minute latitude-longitude and 5-km spatial resolutions are considered extremely fine for such a long history and large domain. Land managers, however, work at resolutions closer to 1 km or less and may desire information more than twice a day. With greater resources it is possible to downscale each product and add accuracy. Until then, we hope users of this first rendition of the VCIS will find value in the information and tools offered from the VCIS Web site.

Acknowledgments

This project was funded through generous support of the Joint Fire Science Program (U.S. Department of the Interior, and U.S. Department of Agriculture, Forest Service). The authors gratefully acknowledge the advice and assistance of Shokoofey Nowbakht and David Dempsey in modifying early versions of the WINFLO model to incorporate spatially varying lapse rates. Special thanks to Steven Hostetler, Rich Fisher, Narasimhan Larkin, and David V. Sandberg for their thoughtful reviews.

English Equivalents

When you know:	Multiply by:	To find:
Meters (m)	3.28	Feet
Kilometers (km)	.6215	Miles
Square kilometers (km^2)	.386	Square miles
Meters per second (m/s)	2.24	Miles per hour
Meters per second (m/s)	1.94	Knots
Square meters per second (m^2/s)	10.76	Square feet per second
KiloPascals (kPa)	10	Millibars
Centigrade (C)	1.8 (and add 32)	Fahrenheit

Literature Cited

Achtemeier, G.L.; Jackson, W.; Hawkins, B. [et al.]. 1998.The smoke dilemma: a head-on collision! In: Transactions of the 63rd North American wildlife and natural resource conference. Washington, DC: Wildlife Management Institute: 415–421.

Alpert, P. 1988. The combined use of three different approaches to obtain the best estimate of meso-surface winds over complex terrain. Boundary-Layer Meteorology. 45: 291–305.

Alpert, P.; Getenio, B. 1988. One-level diagnostic modeling of mesoscale surface winds in complex terrain: I. Comparison with three-dimensional modeling in Israel. Monthly Weather Review. 116(10): 2025–2046.

Alpert, P.; Getenio, B.; Zak-Rosenthal, R. 1988. One-level modeling for diagnosing surface winds over complex terrain: II. Applicability to short-range forecasting. Monthly Weather Review. 116(10): 2407–2461.

Cressman, G.P. 1959. An operational objective analysis system. Monthly Weather Review. 87: 367–374.

Danard, M. 1977. A simple model for mesoscale effects of topography on surface winds. Monthly Weather Review. 105: 572–580.

Dempsey, D.P. 1985. A one-level mesoscale model for diagnosing surface winds in mountainous and coastal regions. Seattle, WA: University of Washington. 182 p. Ph.D. dissertation.

Ferguson, S.A. 2001. Real-time mesoscale model forecasts for fire and smoke management: 2001. In: Proceedings of the fourth symposium on fire and forest meteorology. Boston, MA: American Meteorological Society: 162–167.

Hardy, C.; Ottmar, R.D.; Peterson, J.; Core, J., comps., eds. 2001. Smoke management guide for prescribed and wildland fire: 2001 edition. PMS 420-2. Boise, ID: National Wildfire Coordinating Group. 226 p.

Holzworth, G.C. 1972. Mixing heights, wind speeds, and potential for urban air pollution throughout the contiguous United States. Pub. AP-101. Research Triangle Park, NC: U.S. Environmental Protection Agency, Office of Air Programs. 118 p.

Holzworth, G.C.; Fisher, R.W. 1979. Climatological summaries of the lower few kilometers of rawinsonde observations. Research Triangle Park, NC: U.S. Environmental Protection Agency, Office of Research and Development. 140 p.

Kalnay, E.; Kanamitsu, M.; Kistler, R. [et al.]. 1996. The NCEP/NCAR 40-year reanalysis project. Bulletin of the American Meteorological Society. 77(3): 437–471.

Lipsett M.; Hurley, S.; Ostro, B. 1997. Air pollution and emergency room visits for asthma in Santa Clara County, California. Environmental Health Perspectives. 105(2): 216–222.

Manning, K.W.; Haagenson, P.L. 1992. Data ingest and objective analysis for the PSU/NCAR modeling system: Programs DATAGRID and RAWINS. NCAR Tech. Note NCAR/TN-376+IA. [Boulder, CO]: [National Center for Climate Research]. 209 p.

Mass, C.F.; Dempsey, D.P. 1985. A one-level, mesoscale model for diagnosing surface winds in mountainous and coastal regions. Monthly Weather Review. 113: 1211–1227.

National Climatic Data Center. 1997. Hourly United States weather observations 1990–1995. [CD-ROM]. Asheville, NC: U.S. Department of Commerce, National Oceanic and Atmospheric Administration; Raleigh, NC: U.S. Environmental Protection Agency.

National Renewable Energy Laboratory. 1992. National solar radiation data base 1961-1990. Asheville, NC: National Climatic Data Center; Golden, CO: U.S. Department of Energy. Volumes 1–3.

Neff, W.D.; King, C.W. 1989. The accumulation and pooling of drainage flows in a large basin. Journal of Applied Meteorology. 28: 518–529.

Pasquill, F. 1962. Atmospheric diffusion. London: Van Nostrand. 209 p.

Schwartz, J.; Slater, D.; Larson, T.V. [et al.]. 1993. Particulate air pollution and hospital emergency room visits for asthma in Seattle. American Review of Respiratory Diseases. 147(4): 826–831.

Seaber, P.R.; Kapinos, F.P.; Knapp, G.L. 1987. Hydrologic units maps. Water Supply Paper 2294. [Reston, VA]: U.S. Geological Survey. 63 p.

South Carolina Forestry Commission. 1996. Smoke management guidelines for vegetative debris burning operations in the state of South Carolina. 3rd Printing. Columbia, SC. 19 p.

Speers, P.; Mass, C.F. 1986. Diagnosis and prediction of precipitation in regions of complex terrain. Olympia, WA: Washington State Department of Transportation; WSDOT final report WA-RD-91.1. 166 p.

Turner, D.B. 1964. A dispersion model for an urban area. Journal of Applied Meteorology. 3: 83–91.

U.S. Department of Agriculture, Forest Service. 1976. Southern forestry smoke management guidebook. Gen. Tech. Rep. SE-10. Asheville, NC: Southern Forest Experiment Station. 140 p.

U.S. Department of the Interior, Bureau of Land Management. 1995. Remote automated weather stations (RAWS) and remote environmental monitoring systems (REMS) standards for the United States Department of the Interior, Bureau of Land Management. Boise, ID: National Interagency Fire Center. 37 p.

U.S. Environmental Protection Agency [US EPA]. 1997. National ambient air quality standards for particulate matter; Final Rule. 40 CFR Part 50 [AD-FRL-5725-2] RIN 2060-AE66. Federal Register. 62(138): 38651–38760.

U.S. Environmental Protection Agency [US EPA]. 2001. Office of Air Quality Planning and Standards (OAQPS) Technology Transfer Network (TTN), Support Center for Regulatory Air Models (SCRAM). http://www.epa.gov/scram001. (25 October 2002).

Utah Administrative Code. 2001. Emission standards: general burning. R307-202. http://www.code-co.com/utah/admin/2001/~307202.htm. (25 October 2002).

Wade, D.D.; Lunsford, J.D. 1989. A guide for prescribed fire in southern forests. Tech. Publ. R8-TP11. Atlanta, GA: U.S. Department of Agriculture, Forest Service, Southern Region. 56 p.

Appendix 1: Map Projections

Data Projections

To generate the spatial data components of wind, mixing height, and ventilation index, we used geographic coordinates for the contiguous 48 states and Hawaii, with a grid resolution of 2.5-minute latitude-longitude. The geographic coordinate system creates excessively elongated grid cells above the 50th parallel, however, which cause computational problems for the wind model. Therefore, in Alaska an Albers Conical Equal Area projection was used for generating spatial components, with a grid resolution of 5 km. The following is a summary of map projections used to generate spatial data components of wind, mixing height, and ventilation index:

Contiguous 48 states and Hawaii:

- Projection: Geographic
- Units: Decimal degrees
- Spheroid: WGS84
- Grid size: 2.5 minutes

Alaska:

- Projection: Albers Conical Equal Area
- First standard parallel: 58 00 00
- Second standard parallel: 68 00 00
- Central meridian: -150 00 00
- Origin of the projection: 50 00 00
- False easting: 0
- False northing: 0
- Spheroid: North American Datum 1983
- Grid size: 5000 meters

Web Map Projections

To generate monthly mean maps of the spatial data for display on the Web, we used projections that are common to each region to create maps that look familiar to most users. The following is a summary of map projections used to generate Web maps:

Contiguous 48 states

- Projection: Albers Conical Equal Area
- First standard parallel: 29 30 00
- Second standard parallel: 45 30 00
- Central meridian: -96 00 00
- Origin of the projection: 23 00 00
- False easting: 0
- False northing: 0

- Spheroid: North American Datum 1983
- Grid size: 5000 meters for meteorological data, 2500 meters for background terrain

Alaska

- Projection: Albers Conical Equal Area
- First standard parallel: 58 00 00
- Second standard parallel: 68 00 00
- Central meridian: -150 00 00
- Origin of the projection: 50 00 00
- False easting: 0
- False northing: 0
- Spheroid: North American Datum 1983
- Grid size: 5000 meters for meteorological data, 2500 meters for background terrain

Hawaii

- Projection: Universal Transverse Mercator
- Zone: 4
- Spheroid: North American Datum 1983
- Grid size: 5000 meters for meteorological data, 2500 meters for background terrain

Appendix 2: How to Interpret Graphics

How to Interpret Wind Roses

Wind roses are polar plots that simultaneously display windspeed, wind direction, and relative frequency.

- Windspeeds are shown in meters per second (m/s). One m/s = 1.94 knots = 2.24 miles per hour.
- The percentage of calm winds (<1 m/s) is shown in the center of each wind rose.
- Windspeeds are represented by line thickness and color. Higher windspeeds are indicated by thicker lines and orange to red color.
- The direction that the wind comes from is represented by the angle in which a ray radiates out from the center of the plot. Straight up indicates winds coming from true north.
- Wind frequency is indicated by the length of each line segment of a given thickness and direction. The numerical labels on the concentric circles provide a scale for each graph.

Wind rose example—Figure 20 shows wind frequencies from a site in (a) California and (b) Michigan in August in the afternoon.

- The California site indicates winds predominantly blow from the southwest at this time, and windspeeds frequently exceed 8 m/s. Only 0.32 percent of the winds are calm (less than 1 m/s).
- The Michigan site shows winds prevailing from the south-southeast and south at this time but a significant number of events produce southwest to west winds over the site. Few winds exceed 8 m/s, winds less than 3 m/s occur from all directions, and 4 percent of the winds are calm (less than 1 m/s).

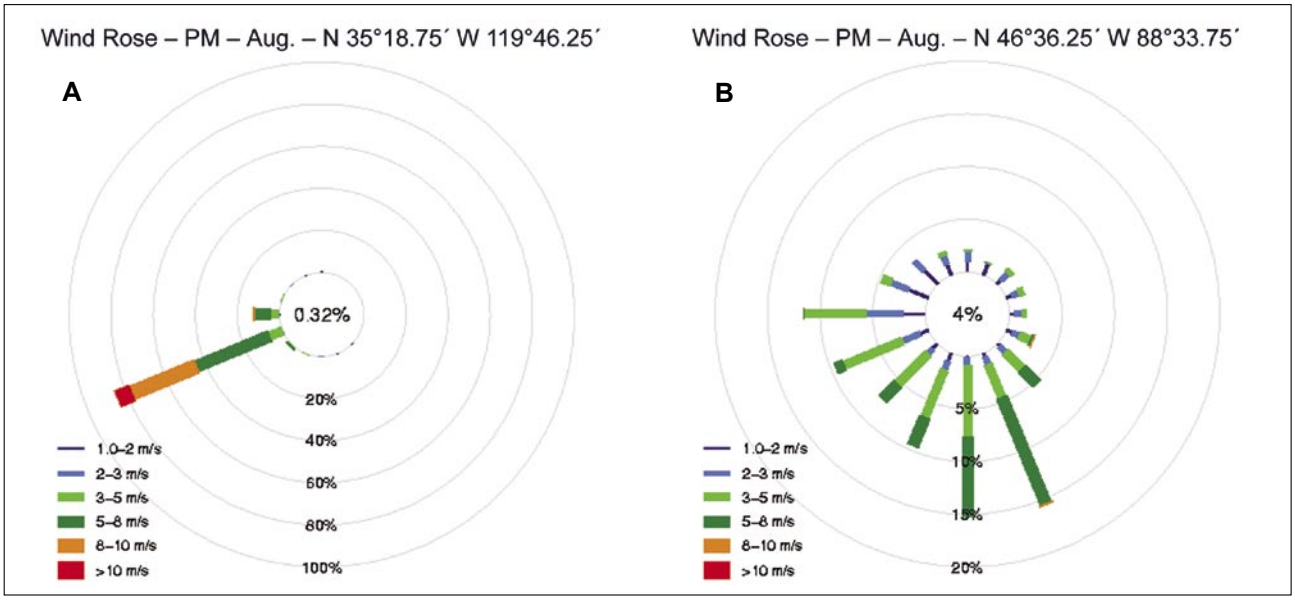

Figure 20—Wind roses from sites in (A) California and (B) Michigan at 0000 universal time coordinated (afternoon) in August. Wind speed is represented by line thickness and color. The direction that the wind comes from is represented by the angle at which the ray radiates out from the center of the plot. Straight up indicates winds coming from the north. The percentage of calm winds (<1 m/s) is shown in the center circle.

How to Interpret Wind Verification Plots

Polar plots of the absolute differences in winds are similar to wind roses in that they simultaneously show differences in speed, direction, and frequency.

- Absolute difference is determined by subtracting each observation from its corresponding modeled value. When observed winds are less than 1 m/s, however, they and the corresponding modeled winds are excluded from difference calculations.
- Some differences may be caused by the model itself, whereas others may be due to the differing resolutions between the model topography and the actual topography. Anemometers are sensitive to small variations in terrain and land use that are not captured in the modeling resolution. See diagrams of surrounding topography and land use that accompany each difference plot to determine this effect.
- Differences between modeled and observed windspeeds are presented as positive values, not distinguishing between overestimation and underestimation. Difference in speed is represented by line thickness and by using the same speed classes as wind roses except that differences (<1 m/s) are not a separate category, causing the thinnest line segments to represent all windspeed differences less than 2 m/s.
- Difference in direction is represented by the angle in which a ray radiates out from the center of the plot. Straight up indicates essentially no difference (within 11.25 degrees). An angle of 90 degrees indicates that the modeled winds differ from the observed winds by 90 degrees in the clockwise direction (i.e., an observed direction of northeast and a modeled direction of southeast).
- Differences are calculated at standard synoptic times of 0Z and 12Z (0000 and 1200 UTC).

Example wind verification—Figure 21 illustrates two sites, one in each row. The top row illustrates a site for which the modeled data match the observed data reasonably well with respect to both direction and speed. This is demonstrated by the long, thin lines pointing toward the top of the absolute differences plot. The second row illustrates a site for which the modeled data do not match the observed data well, as indicated by the shorter, thicker lines pointing in all directions in the absolute differences plot.

- Because 5 percent of the observed winds at the first site were less than 1 m/s, the absolute difference plots correspond to the remaining 95 percent of the observed and modeled winds. Absolute difference at the second site represents 97 percent of the observed and modeled winds.

How to Interpret Box Plots

Box plots simultaneously illustrate variability within and among groups of data.

- The horizontal bar inside each box indicates the median (50^{th} percentile) of the subset.
- The lower and upper limits of the rectangle indicate the quartiles (25^{th} and 75^{th} percentiles, respectively) of the subset.
- The horizontal lines at the ends of the whiskers indicate the extreme values (maximum and minimum) of the subset.

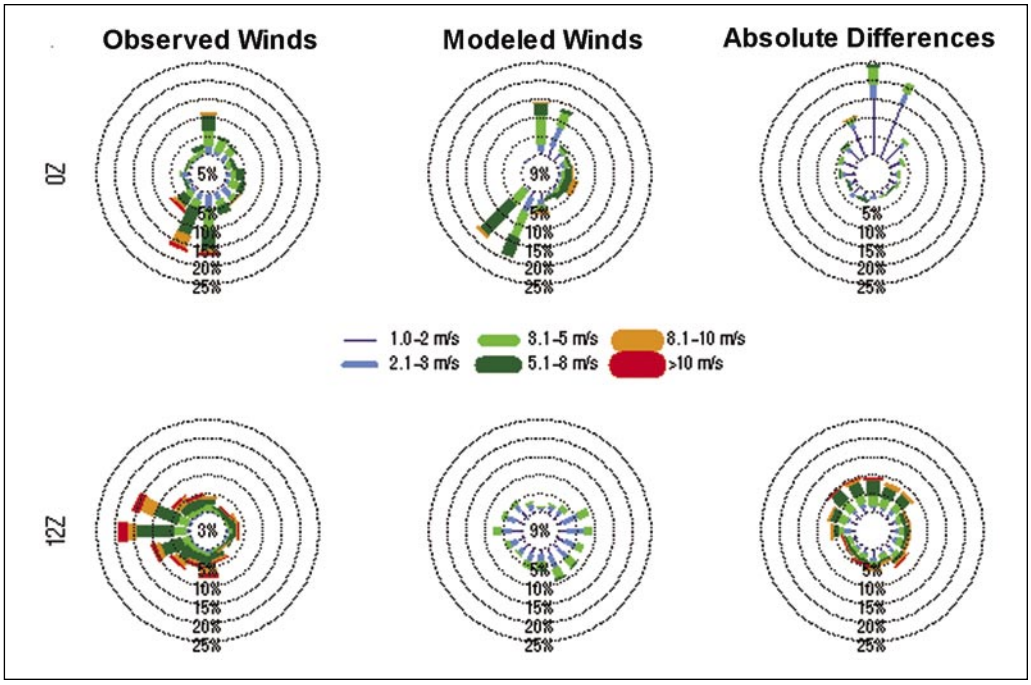

Figure 21—Polar plots of observed and modeled wind, and the absolute difference between modeled and observed for two random sites. The observed and modeled winds are represented as wind roses. The absolute difference shows magnitude of difference by line thickness and angle of difference by the direction in which the ray radiates out from the center of the plot. Straight up indicates direction differences within 11.5 degrees, and a thin line represents speed differences less than 2 m/s.

- The vertical scale of each plot is set to minimize overbearing influence of extreme upper values, and enhance detail in the majority of values. This is done by excluding 0.05 percent of the values that may plot above the highest thousandth tick mark of the graph.

Mixing height—There is a horizontal line at 4000 m on afternoon (PM) box plots and at 1000 m on morning (AM) box plots.

- Interpolated mixing height values sometimes intersect high terrain, creating a belowground value. Mixing can occur to heights well above ground at these places, however, which would allow significant ventilation to occur.
- Because positive mixing height values are needed to calculate ventilation indexes, we set a height to represent the upper limit of mixing whenever interpolated values were less than or equal to zero. The heights were arbitrarily set at 1000 m agl in the morning and 4000 m agl in the afternoon, which approximate maximum values of mixing heights at those times. Unfortunately, the twice-daily time series of historical mixing heights are skewed to these corrected values, especially at high-elevation grid locations.
- Each box plot of mixing height includes a red, horizontal line showing the 1000-m or 4000-m level, where applicable, to help the user determine the effect of the belowground correction.

Example mixing height box plot—Figure 22a illustrates the variability of morning mixing height for a site in Wyoming. The horizontal red line shows the 1000-m correction for belowground mixing height values in the morning. Many times during this month at this site, mixing height is interpolated to a point below ground, and then adjusted to 1000 m. Because there are so many values at 1000 m, at times the 50th percentile and 75th percentile equal 1000 m, causing no box to appear (e.g., April 14 and 16, and 1985, 1987, and 1988).

Figure 22b shows the variability of afternoon mixing height for a site in Minnesota. The horizontal red line shows the 4000 m correction for belowground mixing height values in the afternoon. At this site in this month at this time, mixing height is commonly between 1000 and 3000 m above ground.

- The left side of each figure illustrates the variability within each day of the month across multiple years
- The right side of each figure illustrates the variability within the month from year to year.

Ventilation Index

- Ventilation index box plots use a logarithmic vertical scale. This is to allow more visible detail.
- Color bars on each side of the ventilation index box plots show how the scale relates to mapped categories.
  - Red = poor
  - Yellow = marginal
  - Green = fair
  - White or gray = good

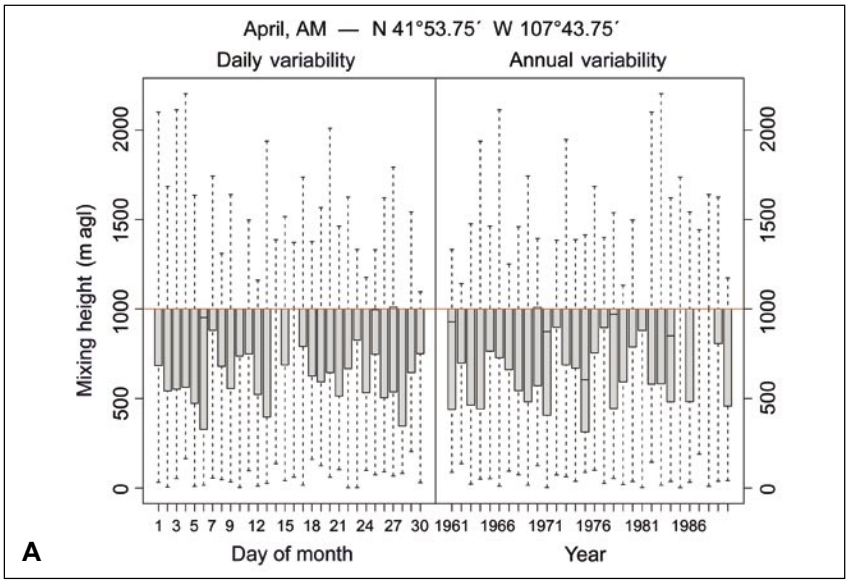

Figure 22—(A) Box plot of morning mixing height in April at a point in Wyoming. The horizontal red line shows the 1000 m correction for belowground mixing height values in the morning. (B) Box plot of afternoon mixing height in April at a point in Minnesota. The horizontal red line shows the 4000 m correction for belowground mixing height values in the afternoon. (C) Box plot of ventilation index for a site in Georgia during the afternoon in April. Color bars indicate poor, marginal, fair, and good classification values (table 4).

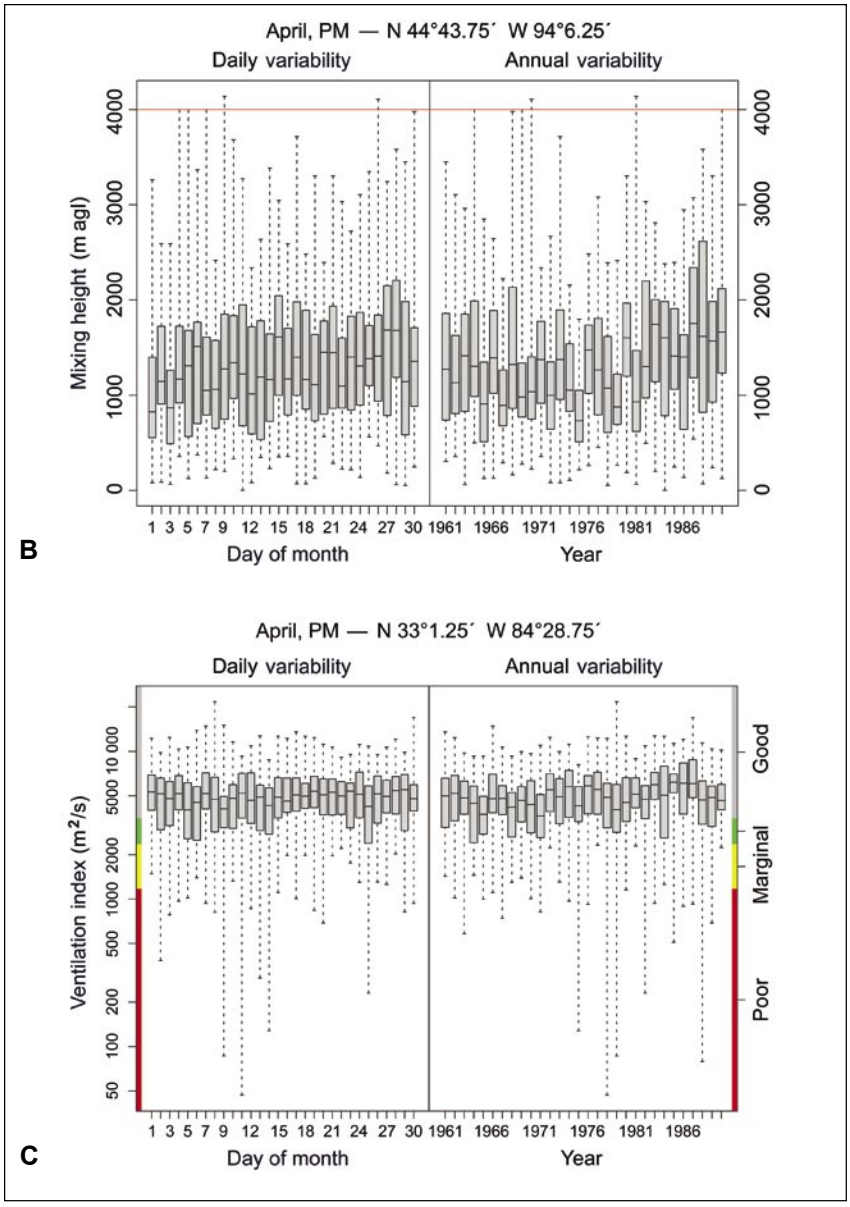

Figure 22—Continued.

Example ventilation index box plot—Figure 22c shows the variability of ventilation index for a site in Georgia in the afternoon. At this site, in this month, and at this time of day, the ventilation index generally is fair, often marginal, and with periods of poor and good ventilation.

- The left side of the figure illustrates the variability within each day of the month across multiple years, whereas the right side of each figure illustrates the variability within the month from year to year.
- Color bars on the figure show that the ventilation index values are mostly good at this site in April.

How to Interpret Maps

Morning monthly mean mixing height—Artifacts in mapped mixing height values appear at the boundaries of local occurrence neighborhoods. This is because local inversion potential is invoked only when certain conditions are met at a nearby surface observation station and adjacent surface stations may have different conditions.

Monthly mean ventilation index—Although ventilation index is calculated as a continuum of values, only four classes are plotted in the monthly mean maps (table 4). This is to facilitate the use of mapped data for assessing potential risk to values of air quality and visibility from wildland fire. The color scale values are half the value of classification schemes commonly used by smoke managers (Hardy et al. 2001). This is because windspeeds at 10 m agl are commonly half of speeds at 40 m agl, a typical height of trajectory winds.

Appendix 3: Summaries of Ventilation Index by Regional Airshed

Box plots show the median, standard deviation, and range of values for each month in each regional airshed in the contiguous 48 states (fig. 23), Alaska (fig. 24), and Hawaii (fig. 25). Airsheds are defined by hydrologic unit code (HUC) code (Seaber et al. 1987) (fig. 19). The contiguous 48 states were divided according to first-order HUC. Second-order HUCs were used to represent airsheds in Alaska. Hawaii is considered a single, separate airshed. Although the ventilation index ranges from zero to well over 70 000 m^2/s, the box plots are truncated at 14 000 m^2/s in the afternoon and 7000 m^2/s in the morning to better illustrate the range of management categories and facilitate cross comparison. Any value above 3525 m^2/s is considered good ventilation potential.

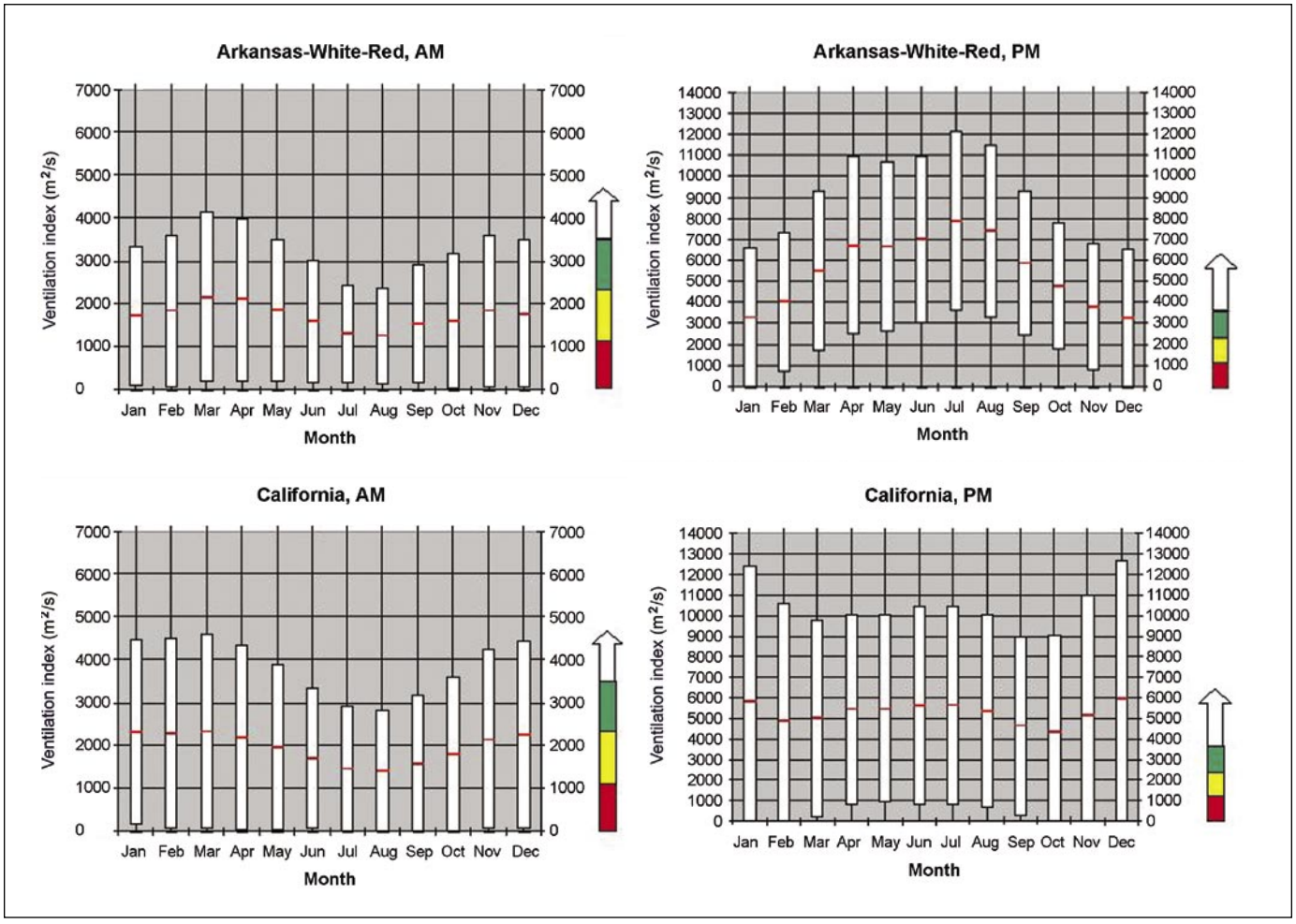

Figure 23—Box plots of ventilation index by month for each regional airshed in the contiguous 48 states. Color bars to the right of each plot indicate categories of poor (red), marginal (yellow), fair (green) and good (white) ventilation potential.

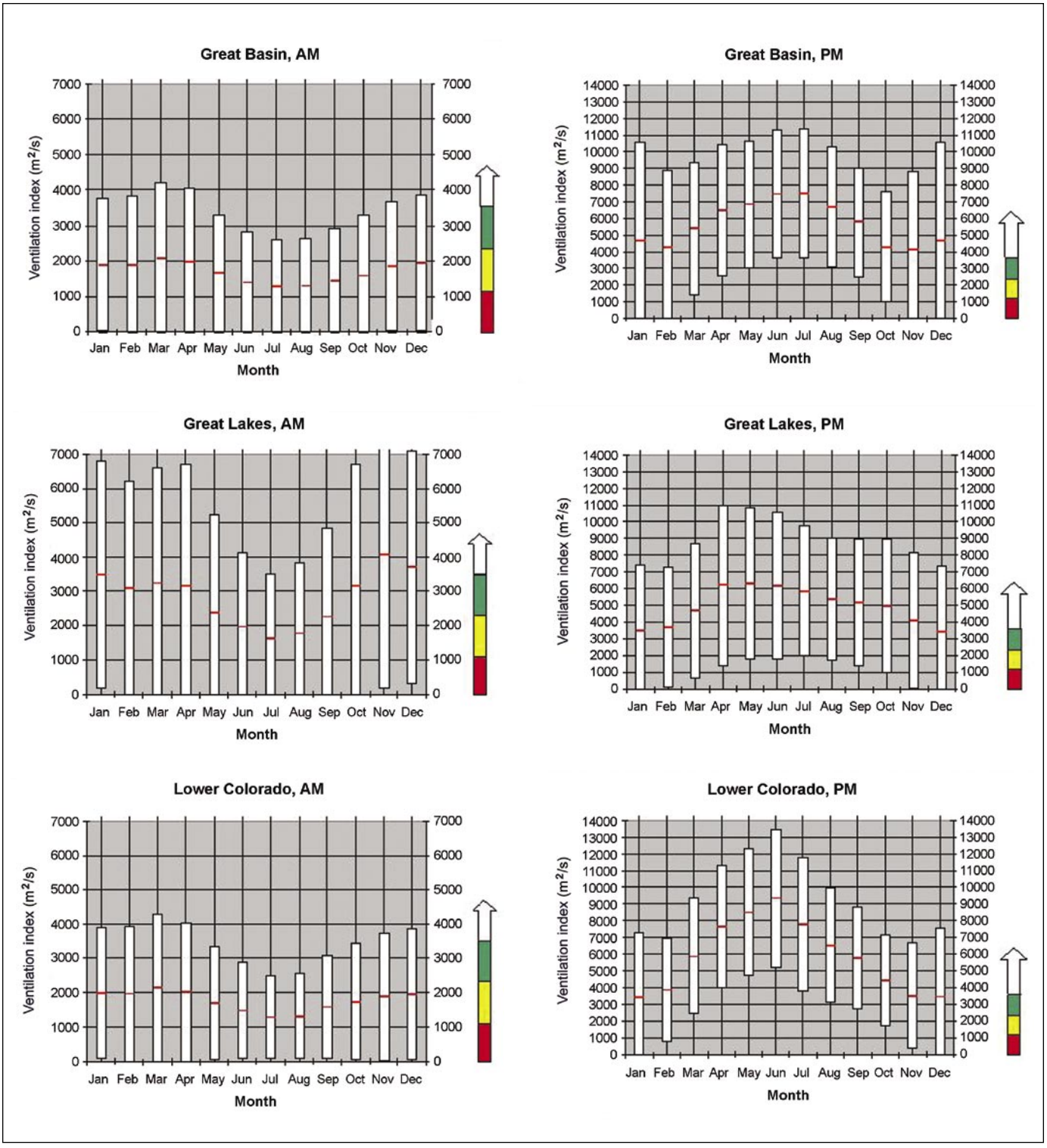

Figure 23—Continued.

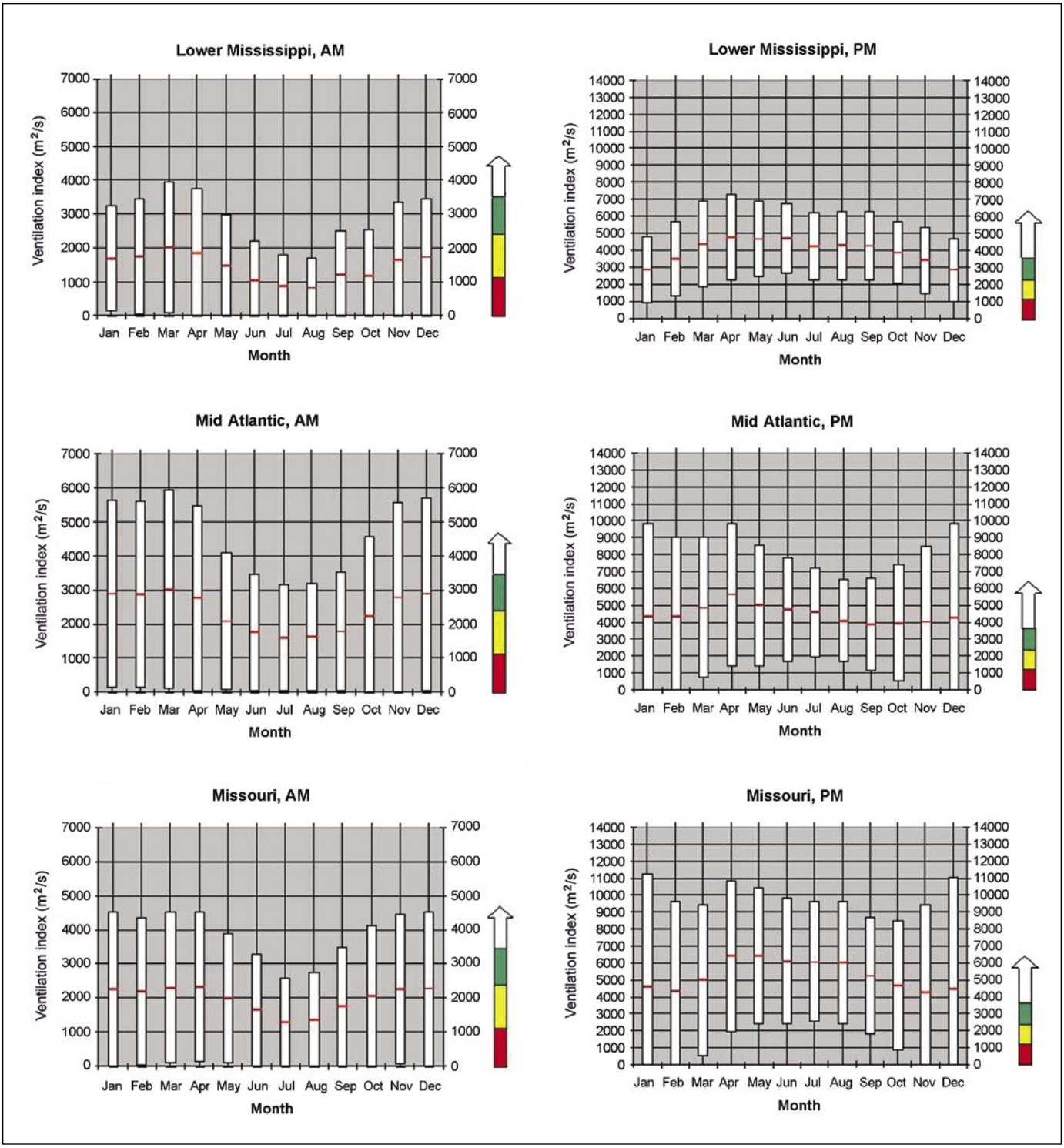

Figure 23—Continued.

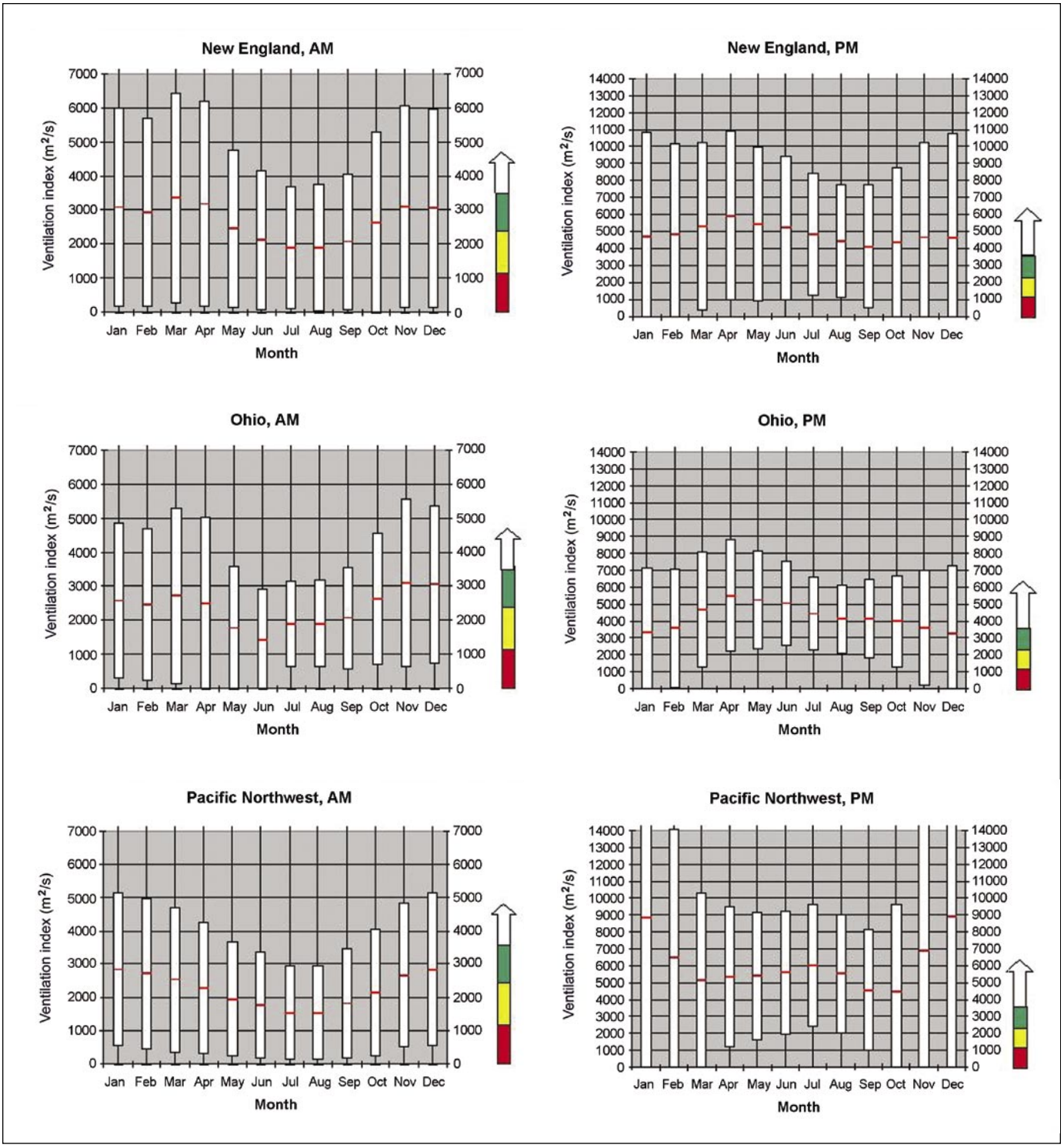

Figure 23—Continued.

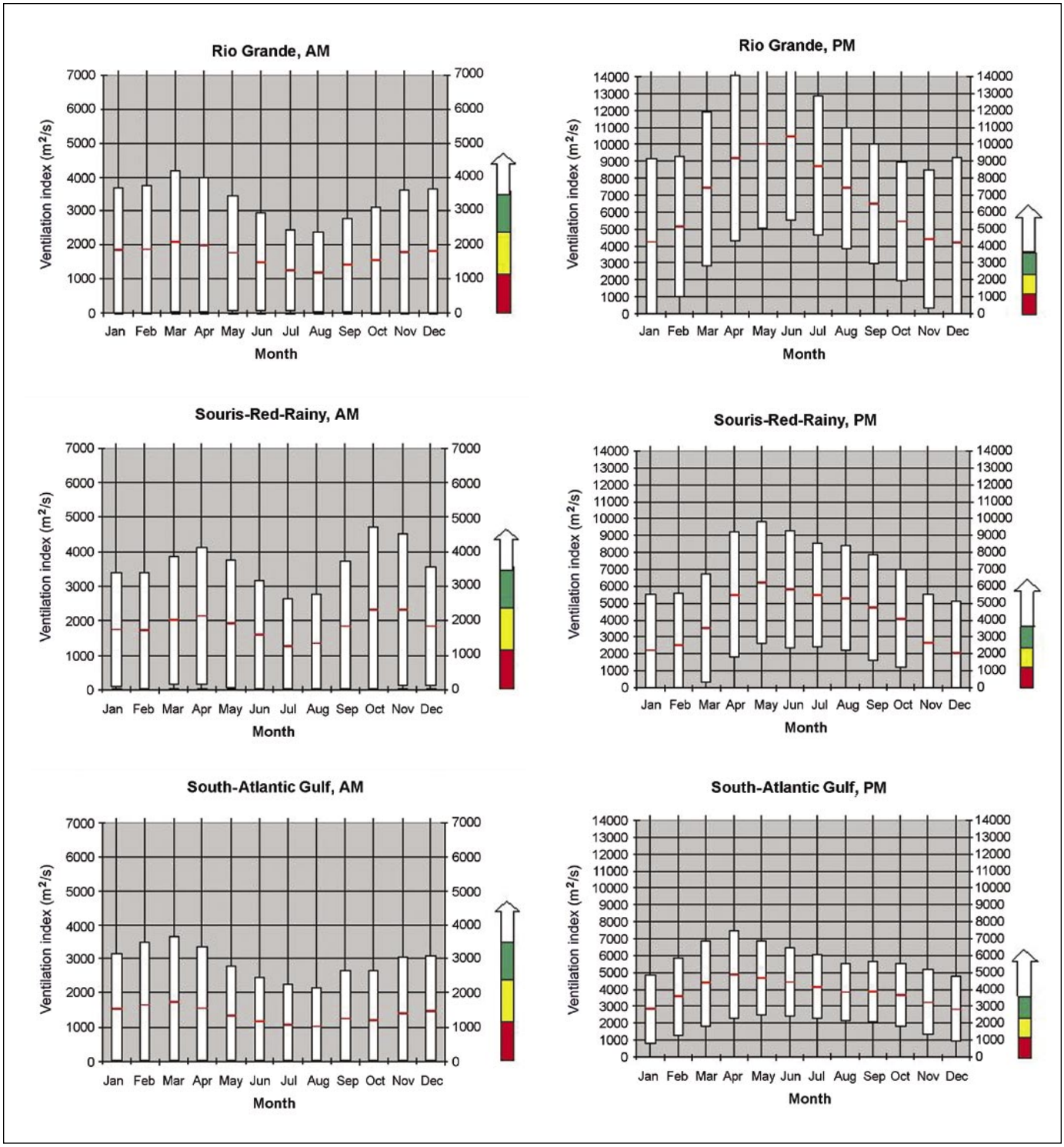

Figure 23—Continued.

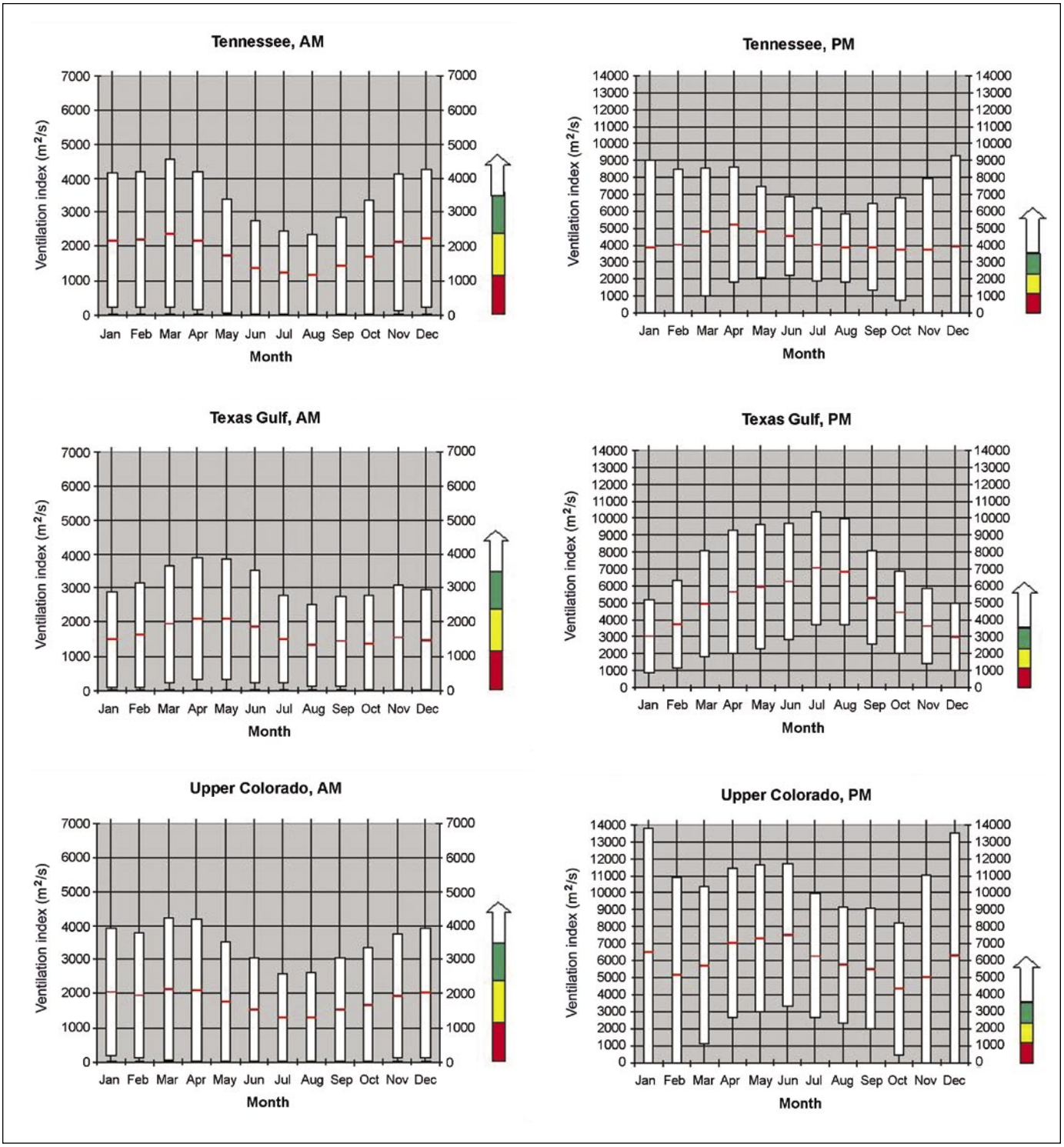

Figure 23—Continued.

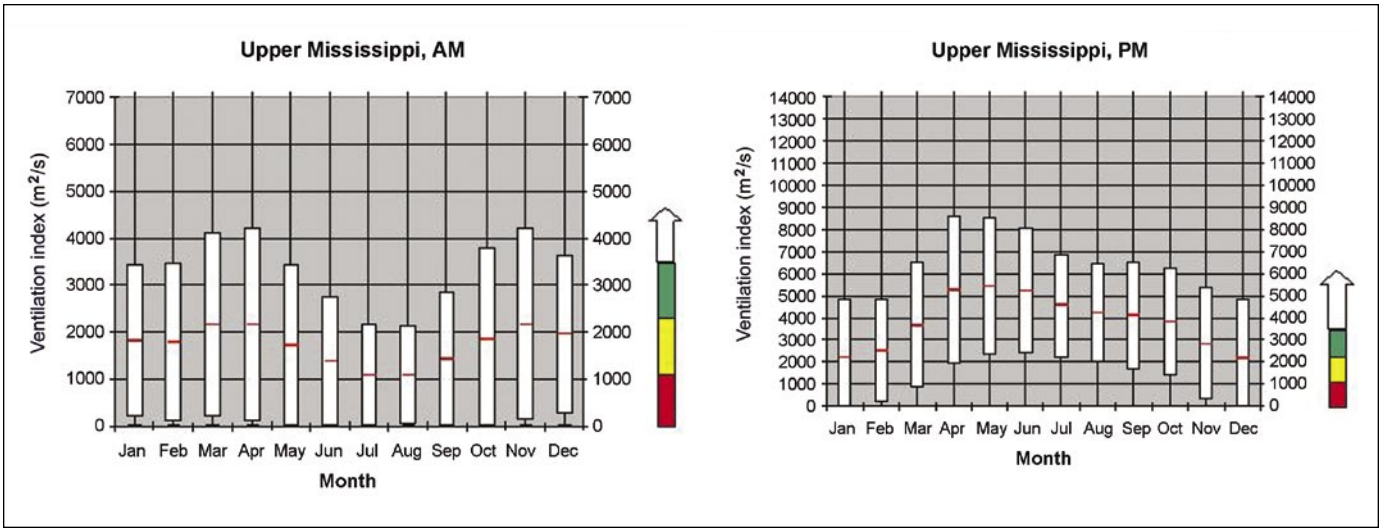

Figure 23—Continued.

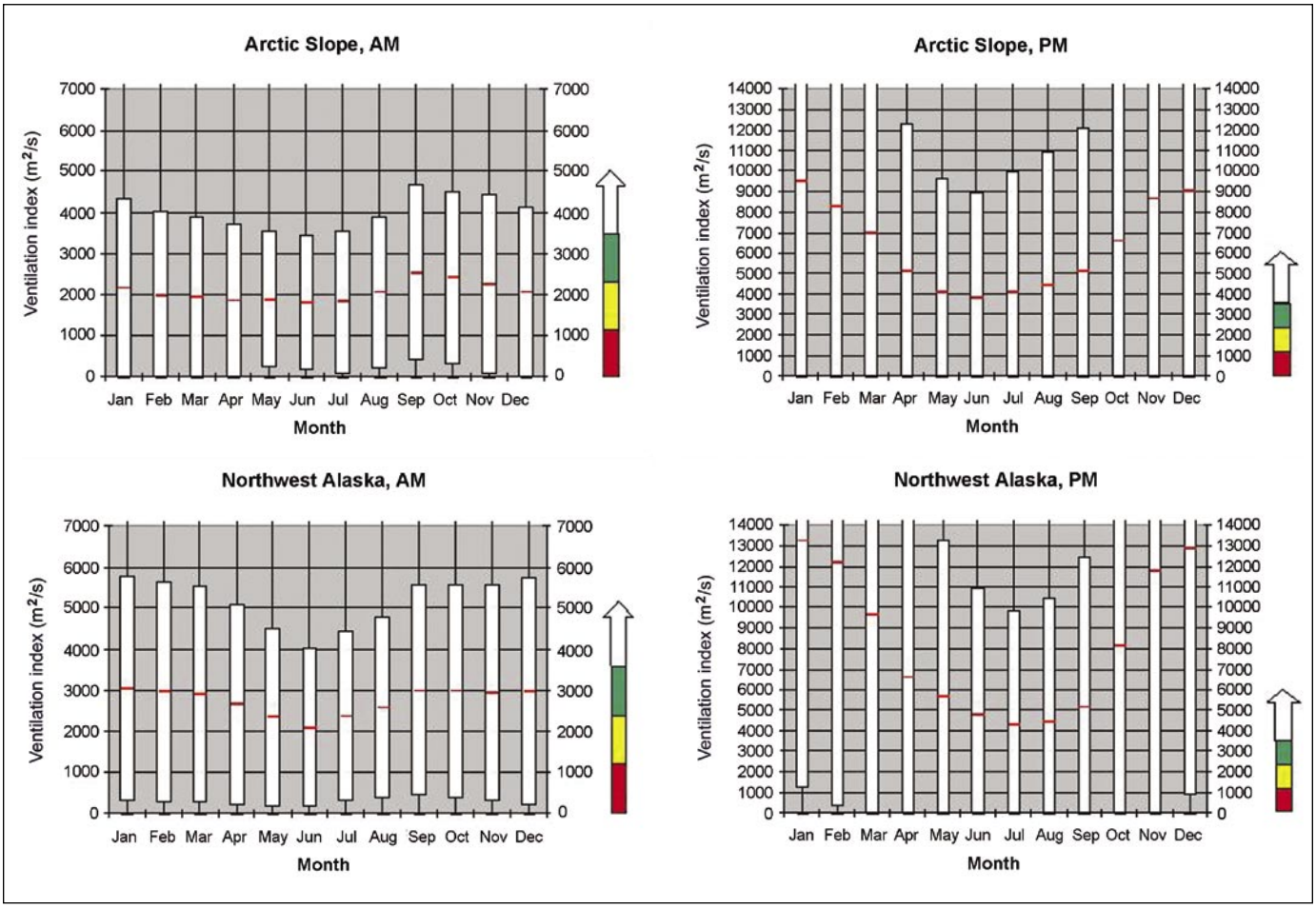

Figure 24—Box plots of ventilation index by month for each regional airshed in Alaska. Color bars to the right of each plot indicate categories of poor (red), marginal (yellow), fair (green) and good (white) ventilation potential.

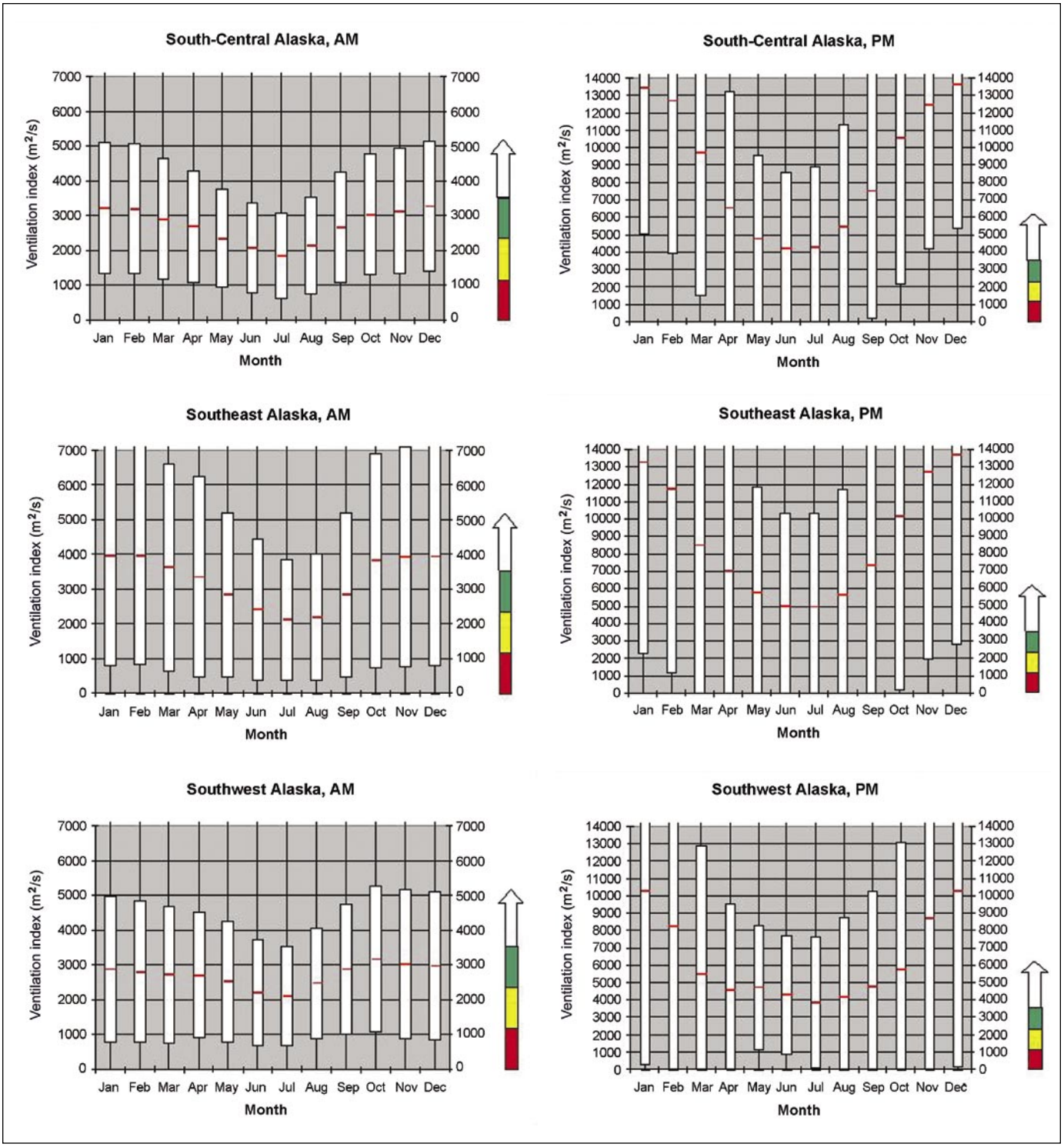

Figure 24—Continued.

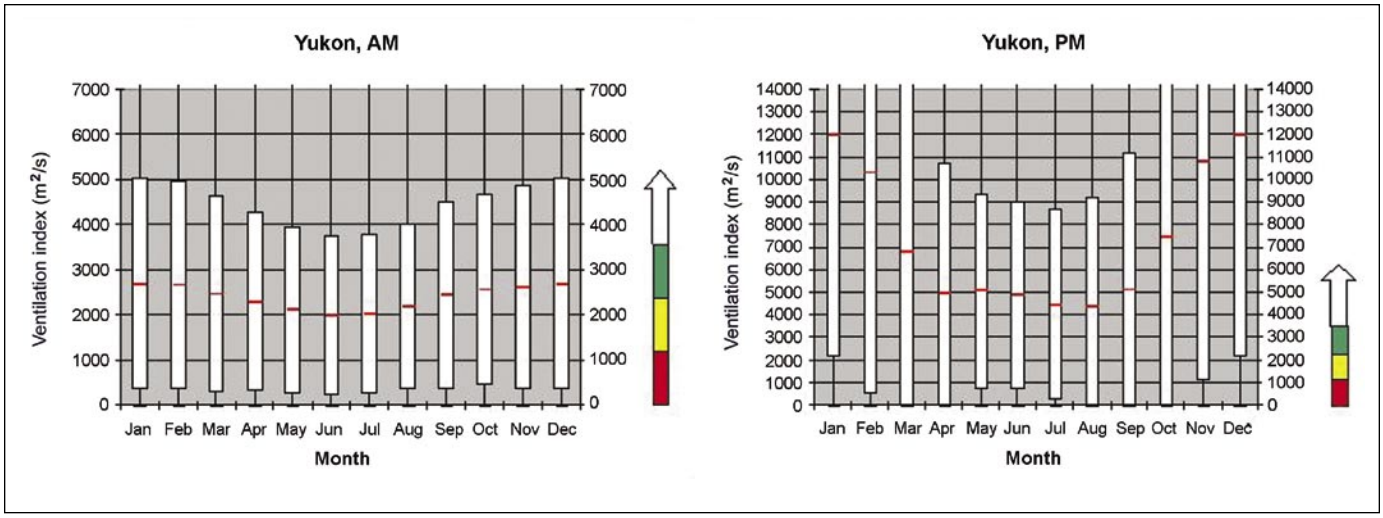

Figure 24—Continued.

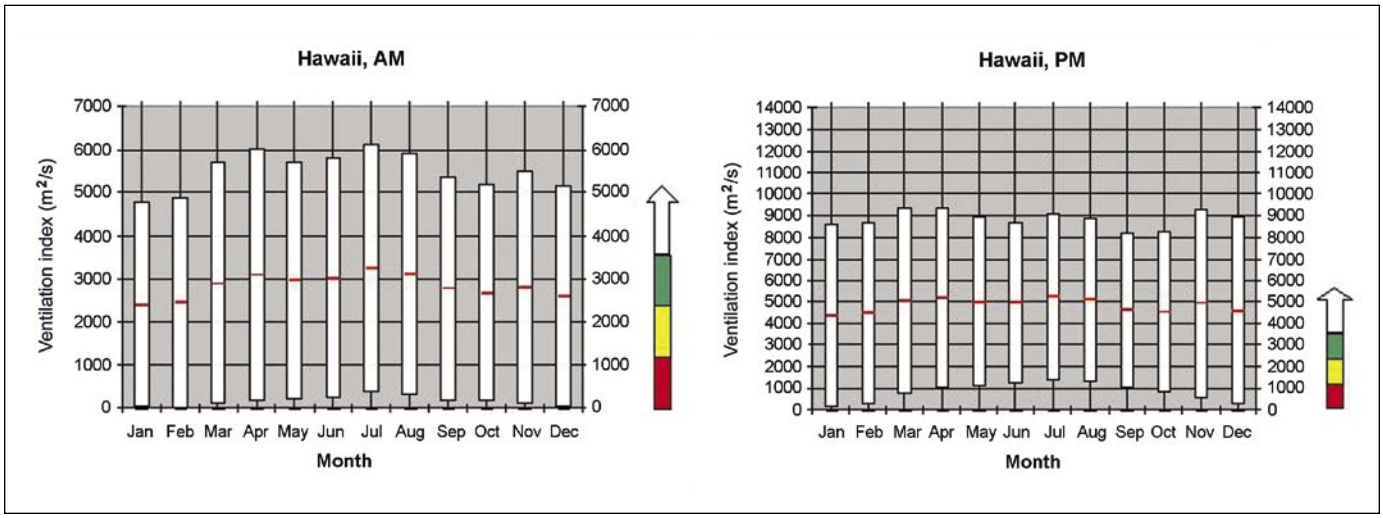

Figure 25—Box plots of ventilation index by month in Hawaii. Color bars to the right of each plot indicate categories of poor (red), marginal (yellow), fair (green) and good (white) ventilation potential.

Appendix 4: The Ventilation Climate Information System Web Site

The ventilation climate information system (VCIS) home page, http://www.fs.fed.us/pnw/fera/vent/, provides access to all documentation, maps, and graphs on ventilation potential in the United States and the associated assessment of air quality and visibility values at risk from wildland fire.

The “Maps and Graphs” button allows access to summary statistics of over 100 gigabytes of data through ArcIMS, the ArcInfo Internet Mapping Service by Environmental Systems Research Institute.[1]

- Alaska, Hawaii, and the contiguous 48 states are separate sites because their maps are projected differently.
- A current browser is needed for the “Maps and Graphs” section (Version 5 or greater of Microsoft Internet Explorer or Version 6 or greater of Netscape Navigator).
- The ArcIMS “Maps and Graphs” opens a separate window from other pages at this site. To return to the VCIS home page, click on the previously open window and use the back button or VENT home link.
- On selecting Alaska, Hawaii, or the contiguous 48 states, enlarge the browser window **before** the site map is loaded. You will be disappointed if you try to enlarge the window after the main map has loaded because the map will remain the size of the opening frame and not fill the extent of the new frame.
- ArcIMS is relatively slow. Therefore, the site works best with a broadband connection to the Internet rather than through a dial-up connection.
- Use the buttons at the top of the “Maps and Graphs” window to navigate through the map frame.


Toggle on or off the inset map.


Zoom in. After selecting this button, you can either (1) click a point on the map to center an interval zoom or (2) define the zoom area by clicking on one corner and holding the left mouse button while dragging open a box. Zooming closer and adding map features allows exact points to be selected. Close zooms also help illustrate the resolution of the data.


Zoom out.


Zoom to full extent.


Go back to last extent.


Pan. Move the map across the screen.


Print. This requires a few moments as it creates a new frame from which you can print just the map and scale or save it to a file.

[1] This use of trade or firm names in this publication is for reader information and does not imply endorsement by the U.S. Department of Agriculture of any product or service.

GET STATS “Get Stats” opens a table of buttons to retrieve statistics on all meteorological variables and all times for a selected point on the map.

- There are over 100 gigabytes of data that the system processes. Therefore, retrieving statistics may require a few moments, especially if using a dial-up connection.
- Click on a button for a time and variable of interest to view a plot of the historical frequency.
- Click on an open graph to reduce its size.
- You can print or save all open graphs by selecting the “Print” button at the top of the table.

- Use the legend on the right to build a map of interest.
  - Select the meteorological base map, monthly mean surface wind, mixing height, or ventilation index.
    - Select the time and month of interest.
    - Check box next to the meteorological window.
    - Click the “Refresh Map” button.
  - Check box next to any of the list of additional features, then click “Refresh Map” button.
- It may be possible to import a map that was built from VCIS into an ArcInfo application. This feature currently is untested.
- To save a map or graph, right click over the image and select “Save Picture As” or “Save Image As.” For maps, this works best from the print window. You can save graphs from any window.

The **Forest Service** of the U.S. Department of Agriculture is dedicated to the principle of multiple use management of the Nation's forest resources for sustained yields of wood, water, forage, wildlife, and recreation. Through forestry research, cooperation with the States and private forest owners, and management of the National Forests and National Grasslands, it strives—as directed by Congress—to provide increasingly greater service to a growing Nation.

Pacific Northwest Research Station

Web site	http://www.fs.fed.us/pnw
Telephone	(503) 808-2592
Publication requests	(503) 808-2138
FAX	(503) 808-2130
E-mail	pnw_pnwpubs@fs.fed.us
Mailing address	Publications Distribution Pacific Northwest Research Station P.O. Box 3890 Portland, OR 97208-3890

U.S. Department of Agriculture
Pacific Northwest Research Station
333 SW First Avenue
P.O. Box 3890
Portland, OR 97208-3890